

The 3-, 4-, and 5-flavor NNLO Parton Distributions Functions from Deep-Inelastic-Scattering Data and at Hadron Colliders

S. Alekhin^{a,b1}, J. Blümlein^{b,2}, S. Klein^{b,3}, S. Moch^{b,4}

^a*Institute for High Energy Physics
142281 Protvino, Moscow Region, Russia*

^b*Deutsches Elektronensynchrotron DESY
Platanenallee 6, D-15738 Zeuthen, Germany*

Abstract

We determine the parton distribution functions (PDFs) in a next-to-next-to-leading order (NNLO) QCD-analysis of the inclusive neutral-current deep-inelastic-scattering (DIS) world data combined with the neutrino-nucleon DIS di-muon data and the fixed-target Drell-Yan data. The PDF-evolution is performed in the $N_f = 3$ fixed-flavor scheme and supplementary sets of PDFs in the 4- and 5-flavor schemes are derived from the results in the 3-flavor scheme using matching conditions. The charm-quark DIS contribution is calculated in a general-mass variable-flavor-number (GMVFN) scheme interpolating between the zero-mass 4-flavor scheme at asymptotically large values of momentum transfer Q^2 and the 3-flavor scheme at the value of $Q^2 = m_c^2$ in a prescription of Buza-Matiounine-Smith-van Neerven (BMSN). The results in the GMVFN scheme are compared with those of the fixed-flavor scheme and other prescriptions used in global fits of PDFs. The strong coupling constant is measured at an accuracy of $\approx 1.5\%$. We obtain at NNLO $\alpha_s(M_Z^2) = 0.1135 \pm 0.0014$ in the fixed-flavor scheme and $\alpha_s(M_Z^2) = 0.1129 \pm 0.0014$ applying the BMSN prescription. The implications for important standard candle and hard scattering processes at hadron colliders are illustrated. Predictions for cross sections of W^\pm - and Z -boson, the top-quark pair- and Higgs-boson production at the Tevatron and the LHC based on the 5-flavor PDFs of the present analysis are provided.

¹**e-mail:** sergey.alekhin@ihep.ru

²**e-mail:** johannes.bluemlein@desy.de

³**e-mail:** sebastian.klein@desy.de

⁴**e-mail:** sven-olaf.moch@desy.de

1 Introduction

For many hard processes at high energies heavy flavor production forms a significant part of the scattering cross section. As it is well known, the scaling violations are different in the massive and massless cases. Therefore, in all precision measurements, a detailed treatment of the heavy flavor contributions is required. This applies, in particular to the extraction of the twist-2 parton distribution functions (PDFs) in deep-inelastic scattering (DIS). In this process $O(25\%)$ of the inclusive cross section in the range of small values of x is due to the production of charm-quarks as measured by the HERA experiments H1 and ZEUS [1, 2]. To perform a consistent QCD-analysis of the DIS world data and other hard scattering data, a next-to-next-to-leading order (NNLO) analysis is required, which includes the 3-loop anomalous dimensions [3] and the corresponding Wilson coefficients [4], in particular those for the heavy flavor contributions. The latter are known at leading order (LO) [5,6] and next-to-leading order (NLO) [7]. In the present paper we restrict the analysis to the NLO heavy flavor corrections. Very recently a series of Mellin moments at NNLO has been calculated in Ref. [8] for the heavy flavor Wilson coefficients of the structure function F_2 , in the region $Q^2 \gtrsim 10 \cdot m_h^2$, where m_h is the heavy quark mass and Q^2 is the momentum transfer squared. Because of the large heavy flavor contribution to F_2 , its correct description is essential in precision measurements of the strong coupling constant α_s and of the PDFs.

At asymptotically large values of Q^2 , the heavy flavor contributions rise like $\alpha_s(Q^2) \ln(Q^2/m_h^2)$. Despite the suppression due to the relatively small value of α_s at large scales, these terms might dominate and therefore their resummation is necessary [6]. It can be easily performed through the renormalization group equations for mass factorization for the process independent contributions defining the so-called variable-flavor-number (VFN) scheme. Thereby heavy quark PDFs are introduced, as e.g. suggested in Ref. [9]. A VFN scheme has to be used in global fits of hadron collider data if the cross sections of the corresponding processes are not available in the 3-flavor scheme. However, since VFN schemes are only applicable at asymptotically large momentum transfers, one has to find a description suitable for lower virtualities Q^2 , which matches with the 3-flavor scheme at the scale $Q^2 = m_h^2$, cf. Ref. [10].

At the same time, the resummed large logarithms occur in the higher order corrections. In the NLO corrections to the massive electro-production coefficient functions [7] the terms up to $\alpha_s^2(Q^2) \ln^2(Q^2/m_h^2)$ are manifest. Therefore the resummation of the remaining large logarithms is much less important as compared to the LO case. Furthermore, in most of the kinematic domain of the DIS experiments the impact of the resummation is insignificant [11]. Eventually, the relevance of the resummation is defined by the precision of the analyzed data and has to be checked in the respective cases. In this paper we study the impact of the heavy flavor corrections on the PDFs extracted from global fits including the most recent neutral-current DIS data. We apply the results of the QCD-analysis to main NNLO hard scattering cross sections, as the W/Z -gauge boson, top-quark pair and Higgs-boson production at hadron colliders.

The paper is organized as follows. In Section 2 we outline the theoretical formalism which describes the heavy quark contributions to DIS structure functions and the formulation of VFN schemes, cf. Refs. [8, 12, 13]. A phenomenological comparison of the fixed-flavor number (FFN)

scheme and different VFN schemes is performed in Section 3 and 4. In Section 4 we present the results of an NNLO PDF-fit to the DIS world data, the fixed-target Drell-Yan- and di-muon data in different schemes using correlated errors to determine the PDF-parameters and $\alpha_s(M_Z^2)$. Precision predictions of PDFs are very essential for all measurements at hadron colliders [14]. Section 5 describes the 3-, 4-, and 5- flavor PDFs generated from the results of our fit and applications to hadron collider phenomenology, such as the scattering cross section of W^\pm - and Z-boson production, the top-quark pair and Higgs-boson cross sections based on the 5-flavor PDFs obtained in the present analysis. Section 6 contains the conclusions.

2 Heavy Quark Contributions: Theoretical Framework

In inclusive DIS, heavy quarks contribute to the final state if we consider extrinsic heavy flavor production only ¹. In fixed-order calculations of the inclusive heavy flavor cross sections in the fixed flavor number scheme (FFNS) for N_f light quarks, one obtains the following representation for the DIS structure functions to NLO in case of single photon exchange [5, 7, 8]

$$F_i^{h,\text{exact}}(N_f, x, Q^2) = \int_x^{x_{\text{max}}} dz \left\{ e_h^2 \left[H_{g,i}(z, Q^2, m_h^2, \mu^2) \frac{x}{z} G\left(N_f, \frac{x}{z}, \mu^2\right) + H_{q,i}^{\text{PS}}(z, Q^2, m_h^2, \mu^2) \frac{x}{z} \Sigma\left(N_f, \frac{x}{z}, \mu^2\right) \right] + \sum_{k=1}^{N_l} e_k^2 L_{g,i}(z, Q^2, m_h^2, \mu^2) \frac{x}{z} G\left(N_f, \frac{x}{z}, \mu^2\right) + L_{q,i}^{\text{NS}}(z, Q^2, m_h^2, \mu^2) \frac{x}{z} f\left(N_f, \frac{x}{z}, \mu^2\right) \right\}, \quad (1)$$

where $i = 2, L$. The functions $H_{g(q),i}$ and $L_{g(q),i}$ denote the massive Wilson coefficients with the photon coupling to the heavy (H) or a light (L) quark line, respectively, $x = Q^2/(2p \cdot q)$ is the Bjorken scaling variable, with q the 4-momentum transfer, p the nucleon momentum, $Q^2 = -q^2$; $x_{\text{max}} = Q^2/(Q^2 + 4m_h^2)$ is production threshold; e_h is the charge of the heavy quark, with $h = c, b$. We introduced a second symbol for the number of the light flavors, N_l , which counts the number of the light quark anti-quark final state pairs associated to the Wilson coefficients $L_{g,i}$. The flavor singlet and non-singlet distributions are given by

$$\Sigma(N_f, x, \mu^2) = \sum_{k=1}^{N_f} [q_k(N_f, x, \mu^2) + \bar{q}_k(N_f, x, \mu^2)], \quad (2)$$

$$f(N_f, x, \mu^2) = \sum_{k=1}^{N_f} e_k^2 [q_k(N_f, x, \mu^2) + \bar{q}_k(N_f, x, \mu^2)], \quad (3)$$

where q_k, \bar{q}_k and G are the light quark, anti-quark and gluon distributions. Here and in the following we identify the factorization and renormalization scales by $\mu = \mu_F = \mu_R$. In open heavy flavor production one usually chooses $\mu^2 = Q^2 + 4m_h^2$, while for the inclusive structure functions one sets $\mu^2 = Q^2$.

¹Potential contributions due to intrinsic charm were limited to be less than 1 % in Ref. [15].

The massive Wilson coefficients in Eq. (1) are available in analytic form at LO [5] and in semi-analytic form at NLO [7]². For $Q^2/m_h^2 \gg 1$ they were given in analytic form to NLO in Refs. [12, 17, 18] and in [8, 19] to NNLO for F_L and F_2 . The NNLO contributions to F_2 are not yet fully available as general expressions in x or the Mellin variable N , since for one part, only a series of Mellin moments at fixed integer values of N has been calculated so far [8]. In the limit $Q^2 \gg m_h^2$, the integration in Eq. (1) extends to $x_{\max} = 1$ and additional soft- and virtual terms contribute to the cross section according to the Kinoshita-Lee-Nauenberg theorem, cf. e.g. [17].

In Ref. [7] the effects due to heavy quark loops in external gluon lines were absorbed for the heavy flavor Wilson coefficients into the strong coupling constant to NLO, which is then to be taken in the corresponding momentum subtraction scheme in Ref. [8]. The necessary changes for α_s in the $\overline{\text{MS}}$ -scheme are discussed in Refs. [8, 12, 13]. In the present paper, we will include the NLO contributions for F_L and F_2 with α_s in the $\overline{\text{MS}}$ -scheme, cf. Ref. [8]. The choice of a MOM scheme always forms an intermediate step, since it applies to the heavy degrees of freedom only. The structure functions also contain the light flavor PDFs and massless Wilson coefficients, the scaling violations of which are governed by $\alpha_s^{\overline{\text{MS}}}$ only. Also, one cannot choose a scheme, which introduces heavy quark mass effects in the strong coupling constant below any heavy flavor threshold.

In the asymptotic region $Q^2 \gg m_h^2$ the Wilson coefficients $L_{g(q),2}$ and $H_{g(q),2}$ for the heavy flavor structure function $F_2^{h,\text{exact}}$ of Eq. (1) can be expressed in terms of the massive operator matrix elements A_{ij} and the massless Wilson coefficients $C_{k,2}$. The former are given by

$$A_{ij}\left(N_f, z, \frac{m_h^2}{\mu^2}\right) = \delta_{ij} + \sum_{n=1}^{\infty} a_s^n(N_f, \mu^2) A_{ij}^{(n)}\left(N_f, z, \frac{m_h^2}{\mu^2}\right), \quad i, j \in \{h, q, g\}; \quad (4)$$

$$A_{ij}^{(1)}\left(z, \frac{m_h^2}{\mu^2}\right) = a_{ij}^{(1,1)}(z) \ln\left(\frac{\mu^2}{m_h^2}\right) + a_{ij}^{(1,0)}(z), \quad (5)$$

$$A_{ij}^{(2)}\left(z, \frac{m_h^2}{\mu^2}\right) = a_{ij}^{(2,2)}(z) \ln^2\left(\frac{\mu^2}{m_h^2}\right) + a_{ij}^{(2,1)}(z) \ln\left(\frac{\mu^2}{m_h^2}\right) + a_{ij}^{(2,0)}(z), \quad (6)$$

cf. Refs. [12, 13, 17, 18, 20]. To NLO the massive OMEs do not depend on N_f . The massless Wilson coefficients for the structure function F_2 are given by

$$C_{k,2}\left(N_f, z, \frac{Q^2}{\mu^2}\right) = \sum_{n=0}^{\infty} a_s^n(N_f, \mu^2) C_{k,2}^{(n)}\left(N_f, z, \frac{Q^2}{\mu^2}\right), \quad k = q, g, \quad (7)$$

cf. Refs. [4, 21]. In case of $C_{q,2}$ we decompose the Wilson coefficients into flavor non-singlet (NS) and pure-singlet (PS) contributions $C_{q,2}^{\text{NS}}$ and $C_{q,2}^{\text{PS}}$. We use the strong coupling constant in the notation $a_s(N_f, \mu^2) = \alpha_s(N_f, \mu^2)/(4\pi)$. At the different heavy flavor thresholds $\mu^2 = m_h^2$, $h = c, b$, matching conditions are employed to $a_s(\mu^2)$, cf. e.g. Ref. [22].

Up to $O(\alpha_s^2)$ the asymptotic expressions for the heavy flavor coefficients $L_{g(q),2}$ and $H_{g(q),2}$

²A fast implementation in Mellin space is given in Ref. [16].

read [8, 17]

$$L_{q,2}^{\text{asmp,NS}} = a_s^2(N_f) \left\{ A_{qq,h}^{(2),\text{NS}} + \left[C_{q,2}^{(2),\text{NS}}(N_f + 1) - C_{q,2}^{(2),\text{NS}}(N_f) \right] \right\}, \quad (8)$$

$$L_{g,2}^{\text{asmp}} = a_s^2(N_f) A_{gg,h}^{(1)} \otimes \frac{1}{N_f} C_{g,2}^{(1)}(N_f), \quad (9)$$

$$H_{q,2}^{\text{asmp,PS}} = a_s^2(N_f) \left[A_{hq}^{(2),\text{PS}} + \frac{1}{N_f} C_{q,2}^{(2),\text{PS}}(N_f) \right], \quad (10)$$

$$H_{g,2}^{\text{asmp}} = a_s(N_f) \left[A_{hg}^{(1)} + \frac{1}{N_f} C_{g,2}^{(1)}(N_f) \right] + a_s^2(N_f) \left\{ A_{hg}^{(2)} + A_{hg}^{(1)} \otimes C_{q,2}^{(1),\text{NS}} \right. \\ \left. + A_{gg,h}^{(1)} \otimes \frac{1}{N_f} C_{g,2}^{(1)}(N_f) + \frac{1}{N_f} C_{g,2}^{(2)}(N_f) \right\}. \quad (11)$$

The symbol \otimes denotes the Mellin convolution

$$[A \otimes B](z) = \int_z^1 \frac{dy}{y} A(y) B\left(\frac{z}{y}\right) \quad (12)$$

and all arguments except of N_f are omitted for brevity. Note that nearly identical graphs contribute to $L_{g,2}^{\text{asmp}}$ and the second last term of $H_{g,2}^{\text{asmp}}$. These are accounted for in different classes due to the final state fermion pair, which consists of the light quarks in the first case and the heavy quark in the second case. Therefore we introduced N_l as a second label for the number of light flavors in the final state, cf. Eq. (1).

The OMEs enter in the matching conditions for the PDFs in the N_f -flavor scheme with the ones for $(N_f + 1)$ massless flavors [12] which are implied by the renormalization group equations. In particular, the NNLO heavy-quark distribution in the $(N_f + 1)$ -flavor scheme at $O(a_s^2)$ reads

$$h^{(1)}(x, \mu^2) + \bar{h}^{(1)}(x, \mu^2) = a_s(N_f + 1, \mu^2) \left[A_{hg}^{(1)}\left(\frac{m_h^2}{\mu^2}\right) \otimes G^{(2)}(N_f, \mu^2) \right](x), \quad (13)$$

$$h^{(2)}(x, \mu^2) + \bar{h}^{(2)}(x, \mu^2) = h^{(1)}(x, \mu^2) + \bar{h}^{(1)}(x, \mu^2) \\ + a_s^2(N_f + 1, \mu^2) \left\{ \left[A_{hg}^{(2)}\left(\frac{m_h^2}{\mu^2}\right) \otimes G^{(2)}(N_f, \mu^2) \right](x) + \left[A_{hq}^{(2),\text{PS}}\left(\frac{m_h^2}{\mu^2}\right) \otimes \Sigma^{(2)}(N_f, \mu^2) \right](x) \right\}, \quad (14)$$

where $G^{(2)}$ and $\Sigma^{(2)}$ are the gluon and flavor singlet distributions, respectively, evolved at NNLO. Likewise, one obtains for the gluon, flavor non-singlet and singlet distributions in the $N_f + 1$ -flavor

scheme up to $O(a_s^2)$

$$\begin{aligned}
G^{(2)}(N_f+1, x, \mu^2) &= G^{(2)}(N_f, x, \mu^2) + a_s(N_f+1, \mu^2) \left[A_{gg,h}^{(1)} \left(\frac{m_h^2}{\mu^2} \right) \otimes G^{(2)}(N_f, \mu^2) \right] (x) \\
&\quad + a_s^2(N_f+1, \mu^2) \left\{ \left[A_{gg,h}^{(2)} \left(\frac{m_h^2}{\mu^2} \right) \otimes G^{(2)}(N_f, \mu^2) \right] (x) \right. \\
&\quad \left. + \left[A_{gq}^{(2)} \left(\frac{m_h^2}{\mu^2} \right) \otimes \Sigma^{(2)}(N_f, \mu^2) \right] (x) \right\}, \tag{15}
\end{aligned}$$

$$\begin{aligned}
\Sigma^{(2)}(N_f+1, x, \mu^2) &= \Sigma^{(2)}(N_f, x, \mu^2) + a_s(N_f+1, \mu^2) \left[A_{hg}^{(1)} \left(\frac{m_h^2}{\mu^2} \right) \otimes G^{(2)}(N_f, \mu^2) \right] (x) \\
&\quad + a_s^2(N_f+1, \mu^2) \left[A_{qq,h}^{(2),NS} \left(\frac{m_h^2}{\mu^2} \right) + A_{hq}^{(2),PS} \left(\frac{m_h^2}{\mu^2} \right) \right] \otimes \Sigma^{(2)}(N_f, \mu^2)(x) \\
&\quad + a_s^2(N_f+1, \mu^2) \left[A_{hg}^{(2)} \left(\frac{m_h^2}{\mu^2} \right) \otimes G^{(2)}(N_f, \mu^2) \right] (x), \tag{16}
\end{aligned}$$

and the light quark and anti-quark distributions are given by

$$\begin{aligned}
q_k^{(2)}(N_f+1, x, \mu^2) + \bar{q}_k^{(2)}(N_f+1, x, \mu^2) \\
= \left[1 + a_s^2(N_f+1, \mu^2) A_{qq,h}^{(2),NS} \left(\frac{m_h^2}{\mu^2} \right) \right] \otimes [q_k^{(2)}(N_f, x, \mu^2) + \bar{q}_k^{(2)}(N_f, x, \mu^2)]. \tag{17}
\end{aligned}$$

These distributions obey momentum conservation

$$\begin{aligned}
1 &= \int_0^1 dx x \left[G(N_f, \mu^2, x) + \Sigma(N_f, \mu^2, x) \right] \\
&= \int_0^1 dx x \left\{ G(N_f+1, \mu^2, x) + \sum_{k=1}^{N_f} [q_k(N_f+1, x, \mu^2) + \bar{q}_k(N_f+1, x, \mu^2)] + h^{(2)}(x, \mu^2) + \bar{h}^{(2)}(x, \mu^2) \right\}. \tag{18}
\end{aligned}$$

Since the OMEs are process independent quantities this property is maintained by the (N_f+1) -flavor PDFs. One may apply these PDFs in a hard scattering process for large enough scales $\mu_F^2 \gg m_h^2$, where the power corrections are negligible. In particular, the heavy flavor structure function F_2 is defined in the (N_f+1) -flavor scheme as the convolution of the (N_f+1) -flavor PDFs with the massless Wilson coefficients $C_{q(g),2}$. This representation is the so-called zero mass VFN (ZMVFN) scheme expression, which is applicable only in the asymptotic region.

The heavy flavor part of F_2 in the region $Q^2 \gg m_h^2$ for $N_f + 1$ flavors up to $O(\alpha_s^2)$ is given by

$$\begin{aligned}
F_2^{h,\text{ZMVFN}}(N_f + 1, x, Q^2) &= xe_h^2 \left\{ h^{(2)}(x, \mu^2) + \bar{h}^{(2)}(x, \mu^2) \right. \\
&+ a_s(N_f + 1, \mu^2) \left[\frac{1}{N_f} C_{g,2}^{(1)} \left(N_f, \frac{Q^2}{\mu^2} \right) \otimes G^{(2)}(N_f, \mu^2) \right] (x) \\
&+ a_s^2(N_f + 1, \mu^2) \left[A_{gg,h}^{(1)} \left(\frac{m_h^2}{\mu^2} \right) \otimes \frac{1}{N_f} C_{g,2}^{(1)} \left(N_f, \frac{Q^2}{\mu^2} \right) \otimes G^{(2)}(N_f, \mu^2) \right] (x) \\
&+ a_s(N_f + 1, \mu^2) \left[C_{q,2}^{(1),\text{NS}} \left(\frac{Q^2}{\mu^2} \right) \otimes [h^{(1)}(\mu^2) + \bar{h}^{(1)}(\mu^2)] \right] (x) \\
&+ \frac{1}{N_f} a_s^2(N_f + 1, \mu^2) \left(\left[C_{q,2}^{(2),\text{PS}} \left(N_f, \frac{Q^2}{\mu^2} \right) \otimes \Sigma^{(2)}(N_f, \mu^2) \right] (x) + \left[C_{g,2}^{(2)} \left(N_f, \frac{Q^2}{\mu^2} \right) \otimes G^{(2)}(N_f, \mu^2) \right] (x) \right) \Big\} \\
&+ x \frac{1}{N_f} \sum_{k=1}^{N_l} e_k^2 a_s^2(N_f + 1, \mu^2) \left[A_{gg,h}^{(1)} \left(\frac{m_h^2}{\mu^2} \right) \otimes C_{g,2}^{(1)} \left(N_f, \frac{Q^2}{\mu^2} \right) \otimes G^{(2)}(N_f, \mu^2) \right] (x) \\
&+ x a_s^2(N_f + 1, \mu^2) \left[\left(A_{qq,h}^{(2),\text{NS}} \left(\frac{m_h^2}{\mu^2} \right) + C_{q,2}^{(2),\text{NS}} \left(N_f + 1, \frac{Q^2}{\mu^2} \right) - C_{q,2}^{(2),\text{NS}} \left(N_f, \frac{Q^2}{\mu^2} \right) \right) \otimes f(N_f, \mu^2) \right] (x).
\end{aligned} \tag{19}$$

At this point we would briefly like to comment on the longitudinal structure function F_L . As a matter of fact, the above concept of a ZMVFN scheme cannot be directly applied to the heavy flavor component of F_L even in the asymptotic regime of $Q^2 \gg m_h^2$; e.g. at $O(\alpha_s)$, similarly to Eq. (19), one obtains

$$F_L^{h,\text{asympt}}(N_f + 1, x, Q^2) = a_s(N_f + 1, \mu^2) e_h^2 \left[C_{g,L}^{(1)} \left(\frac{Q^2}{\mu^2} \right) \otimes G(N_f, \mu^2) \right] (x), \tag{20}$$

Here, the gluon density is convoluted with the LO gluon Wilson coefficient $C_{g,L}^{(1)}$ but not a splitting function, because unlike the case of F_2 no collinear logarithm emerges. The example illustrates that a detailed renormalization group analysis is a necessary prerequisite to the use of heavy quark densities even in the asymptotic region, cf. Ref. [12].

3 Comparison of the 3- and the 4-Flavor Schemes

At $O(\alpha_s^l)$ the universal contribution (referring to the massive OMEs only) to the heavy flavor singlet contribution to F_2 is given by

$$\widehat{F}_2^{h,(l)}(N_f = 4, x, Q^2) = e_h^2 x [h^{(l)}(x, \mu^2) + \bar{h}^{(l)}(x, \mu^2)], \quad l = 1, 2. \tag{21}$$

It vanishes for $\widehat{F}_2^{h,(1)}$ at $\mu^2 = m_h^2$, since $a_{hg}^{(1,0)} = 0$, cf. Eq. (4), and it is negative for $\mu^2 < m_h^2$. However, the 1st order heavy quark contribution to the structure function F_2 is positive, since

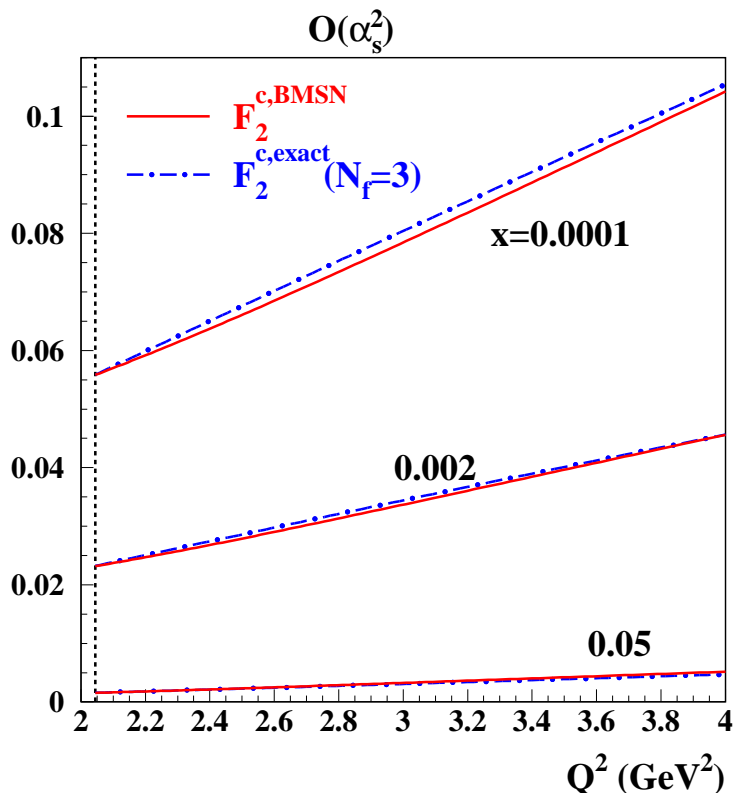


Figure 1: Matching of $F_2^{c,BMSN}(N_f = 4, x, Q^2)$ (solid lines) with $F_2^{c,exact}(N_f = 3, x, Q^2)$ (dash-dotted lines) at small Q^2 in $O(\alpha_s^2)$. The vertical line denotes the position of the charm-quark mass $m_c = 1.43$ GeV.

the μ^2 dependence is canceled by a corresponding logarithm $\propto \ln(Q^2/\mu^2)$ in the massless Wilson coefficient $C_{g,2}^{(1)}$ in Eq.(19). Despite that in the 3-flavor scheme the heavy quark contribution to the DIS structure functions also falls at small Q^2 , it is present down to the photo-production limit. At $O(\alpha_s^2)$ the agreement between the two schemes at low Q^2 is even worse since the term $a_{hg}^{(2,0)}$ is negative which implies $\widehat{F}_i^{h,(2)}(N_f = 4, x, Q^2) < 0$ because the gluon contribution dominates over the pure-singlet part numerically. The impact of the large-log resummation is negligible at small scales Q^2 and any reasonable scheme must reproduce the 3-flavor scheme. Therefore, at low values of Q^2 the ZMVFN scheme is not applicable. It has to be modified according to practical purposes. VFN schemes with such modifications are called general-mass variable-flavor-number (GMVFN) schemes, in contrast to the ZMVFN scheme. A particular form of the GMVFN scheme cannot be derived from first principles in a unique way, but is subject to the corresponding prescription. Consistent schemes have to obey renormalization group equations to not violate the running of the coupling constant and masses, and to obey correct scale evolution. As a general requirement any such prescription should provide a continuous transition from the 3-flavor scheme at low values of μ^2 to the 4-flavor scheme at large scales.

An early formulation of a GMVFN scheme by Aivazis-Collins-Olness-Tung (ACOT) [9] does not allow a smooth matching with the 3-flavor scheme at small scales Q^2 . In the ACOT scheme, the

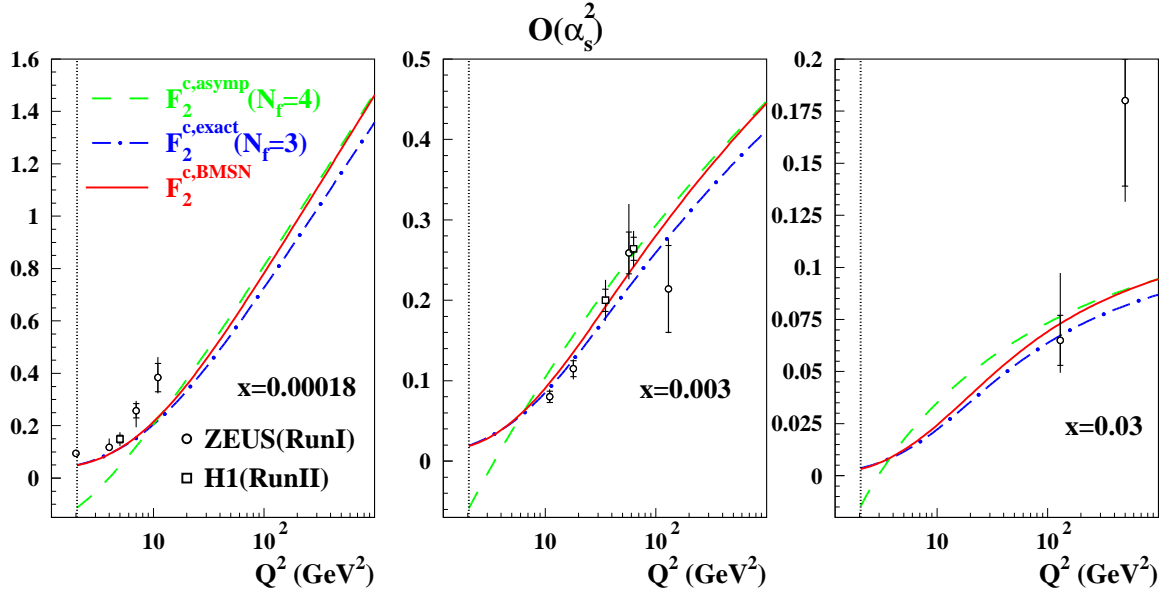


Figure 2: Comparison of F_2^c in different schemes to H1- and ZEUS-data. Solid lines: GMVFN scheme in the BMSN prescription, dash-dotted lines: 3-flavor scheme, dashed lines: 4-flavor scheme. The vertical dotted line denotes the position of the charm-quark mass $m_c = 1.43$ GeV.

slope in Q^2 turns out to be too large. Later the so-called Thorne-Roberts (TR) scheme overcoming this shortcoming was suggested [23]. However, beyond NLO this scheme is very involved and its numerical implementation is problematic [24]. Recently, the early ACOT prescription has been modified in order to improve the behavior at low values of Q^2 [25]. This modified description, the so-called ACOT(χ) scheme, is used in particular at NNLO in Ref. [26]. Another GMVFN prescription, which was suggested earlier by Buza-Matiounine-Smith-van Neerven (BMSN) [12] for F_2^h , is defined by

$$F_2^{h,\text{BMSN}}(N_f + 1, x, Q^2) = F_2^{h,\text{exact}}(N_f, x, Q^2) + F_2^{h,\text{ZMVFN}}(N_f + 1, x, Q^2) - F_2^{h,\text{asympt}}(N_f, x, Q^2), \quad (22)$$

with $N_f = 3$ for $h = c$.

Note that the difference of the last two terms in Eq. (22) depends on N_f through the strong coupling constant only, which is a specific feature up to NLO. For the choice of $\mu^2 = Q^2$ the asymptotic terms cancel at $Q^2 = m_h^2$ in Eq. (22). In this limit $F_2^{h,\text{BMSN}}(N_f = 4)$ reproduces the result in the 3-flavor scheme. Moreover, $F_2^{h,\text{BMSN}}(N_f = 4)$ matches with the 3-flavor scheme smoothly as shown in Figure 1. Minor kinks between $F_2^{h,\text{BMSN}}(N_f = 4)$ and $F_2^{h,\text{exact}}(N_f = 3)$ stem from the matching of $\alpha_s(N_f, \mu^2)$ at $\mu^2 = m_h^2$. It appears since the matching condition for $\alpha_s(N_f, \mu^2)$ does not provide a continuous but not a smooth transition at the flavor thresholds. The numerical impact of this kink is marginal in the analysis of the current data. At large Q^2 the asymptotic expression $F_2^{h,\text{asympt}}(N_f = 3)$ cancels the term $F_2^{h,\text{exact}}(N_f = 3)$ in Eq. (22) and $F_2^{h,\text{BMSN}}(N_f = 4)$ reproduces the result in the ZMVFN scheme. The cancellation is not perfect due to the difference in the upper limit of integration in Eq. (1) and the expression for the ZMVFN scheme, which affects

only the non-singlet Compton-type contribution given by the coefficient functions $L_{q,i}^{\text{NS}}$. For the 3-flavor expression of Eq. (1), this term rises as $\ln^3(Q^2/m_h^2)$ at large Q^2 . In the asymptotic limit of Ref. [17] the corresponding singular contribution is washed out in $L_{q,2}^{\text{asympt,NS}}$. As a result, there remains a contribution $\sim \ln^3(Q^2/m_h^2)$ in the difference of $F_2^{h,\text{exact}}(N_f = 3)$ and $F_2^{h,\text{asympt}}(N_f = 3)$. This mismatch is caused by a well-known soft and virtual term, which occurs in the inclusive analysis for large arguments of the Wilson coefficient and is easily corrected, cf. Ref. [17,27]. On the other hand, the non-singlet contribution to heavy quark electro-production is numerically very small and the term $\sim \ln^3(Q^2/m_h^2)$ is apparent only at very large values of Q^2 and relatively large x . The accuracy of realistic data at this kinematics is rather poor and even for the definition of Eq. (1) the impact of the mismatch between $F_2^{h,\text{exact}}(N_f = 3)$ and $F_2^{h,\text{asympt}}(N_f = 3)$ turns out to be marginal in the data analysis.

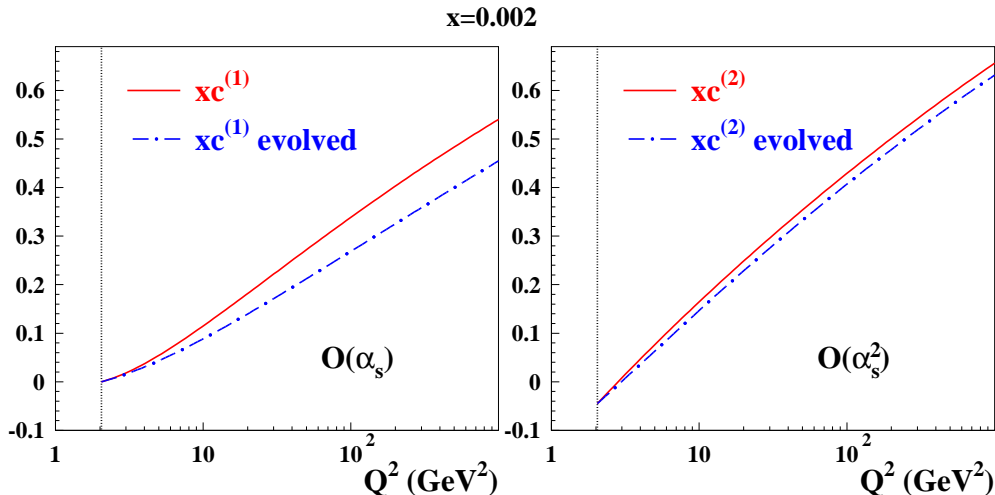


Figure 3: The c -quark distributions calculated using the fixed-order relation Eqs. (14,13) (solid lines) compared to the result in the 4-flavor scheme evolving from m_c^2 and using Eqs. (14,13) as boundary condition (dash-dotted lines) at $O(\alpha_s)$ (left panel) and at $O(\alpha_s^2)$ (right panel).

A representative set of the ZEUS- and H1-data [2, 28] on F_2^c is compared to $F_2^{c,\text{BMSN}}(N_f = 4)$, $F_2^{c,\text{exact}}(N_f = 3)$, and $F_2^{c,\text{ZMVFN}}(N_f = 4)$ in Figure 2. The 3-flavor PDFs used in this comparison are evolved starting from $m_c = 1.43$ GeV with the input given by the MRST2001 PDFs of Ref. [29]. Because of the kinematic constraints, at $x \sim 0.0001$ only the values of $Q^2 \lesssim 10$ GeV² are available in the data. At such low scales the calculation in the 3-flavor and BMSN scheme yield practically the same results. At $x \sim 0.01$ the typical values of Q^2 are much bigger. In this kinematic region, the BMSN scheme yields a larger contribution than obtained in the 3-flavor scheme. However, the uncertainties in the data are still quite large due to limited statistics. The comparison of the calculations with the data is rather insensitive to the choice of scheme. The non-singlet term in Eq. (1) is not taken into account in the comparisons shown in Figure 2. Its impact is most significant at large values of x and Q^2 , but even in this case, it is much smaller than the data uncertainty. For intermediate values of $x \sim 0.001$, a combination of these two cases is observed: at large Q^2 the uncertainties in the data do not allow to distinguish between both schemes, while at small Q^2

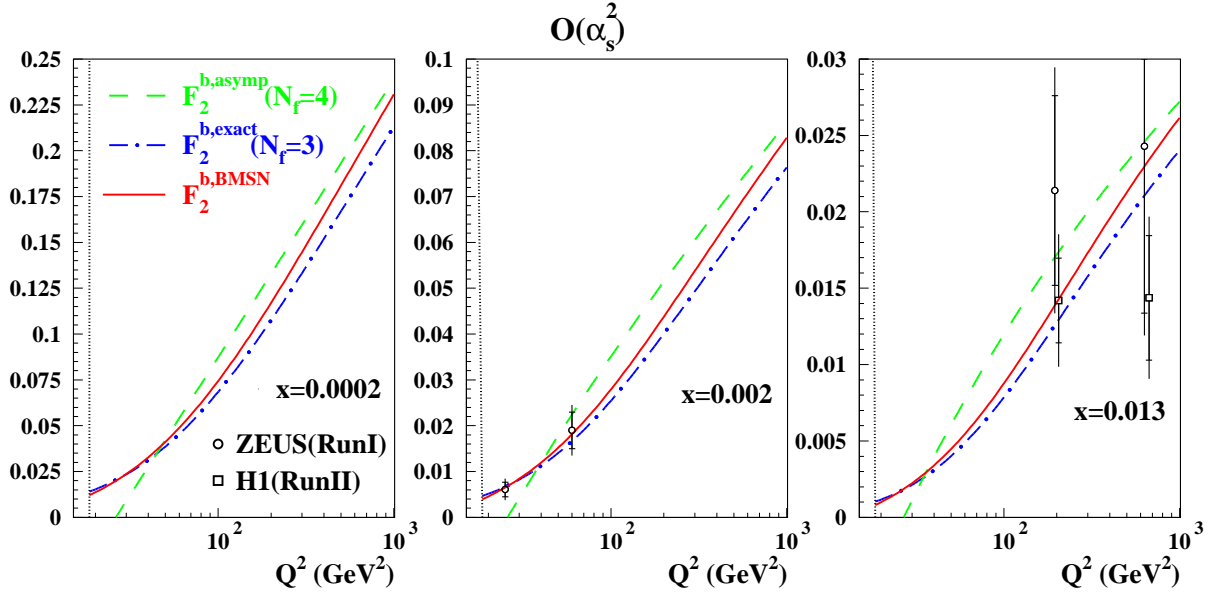


Figure 4: Comparison of predictions in different schemes to ZEUS- and H1-data on $F_2^b(x, Q^2)$. The notations are the same as in Figure 2. The vertical dotted line marks the position of $m_b = 4.3$ GeV.

the numerical difference between the 3-flavor and the BMSN scheme calculations is very small. Summarizing, for the analysis of realistic data on F_2^c , the BMSN scheme is very similar to the 3-flavor scheme. This is not a particular feature of the BMSN prescription, since the difference between 3- and 4-flavor schemes at large Q^2 is also smaller than the uncertainties in the available data and, once the smooth matching is provided, a GMVFN scheme must be close to the 3-flavor one at small Q^2 . This conclusion is in agreement with the results of Ref. [30]. It derives from the fact that once the $O(\alpha_s^2)$ corrections are taken into account the need of a large-log resummation is thus greatly reduced, which is well known for a long time, cf. Ref. [11]. In Figure 3 the c -quark distribution defined in Eq. (13,14) is compared to the one evolved in the 4-flavor scheme starting from the scale of m_c using Eqs. (13,14) as boundary conditions. The former is derived from fixed-order perturbation theory, while for the latter resummation is performed through the evolution equations. At $O(\alpha_s)$ the difference between these two approaches is significant indeed, however, at $O(\alpha_s^2)$ it is much smaller, and quite unimportant for realistic kinematics.

As evident from Figure 2 the scheme choice cannot resolve observed discrepancies between data and the theoretical predictions to NLO. Given the mass of the charm quark and the PDFs determined in inclusive analyses, higher order QCD corrections are needed. In particular, at small x and Q^2 , the partial $O(\alpha_s^3)$ corrections to the massive Wilson coefficient $H_{g,2}$ obtained through threshold resummation [31] give a significant contribution to F_2^c and greatly improve the agreement to the data [32]. In this kinematic region, the integral of Eq. (1) is mostly sensitive to the threshold of heavy quark production and the approximate form of $H_{g,2}$ derived in Ref. [32] is sufficient. At large values of Q^2 , the threshold approximation is inapplicable, and a complete NNLO calculation is required, cf. Ref. [8]. For b -quark production the resummation effects are less important since

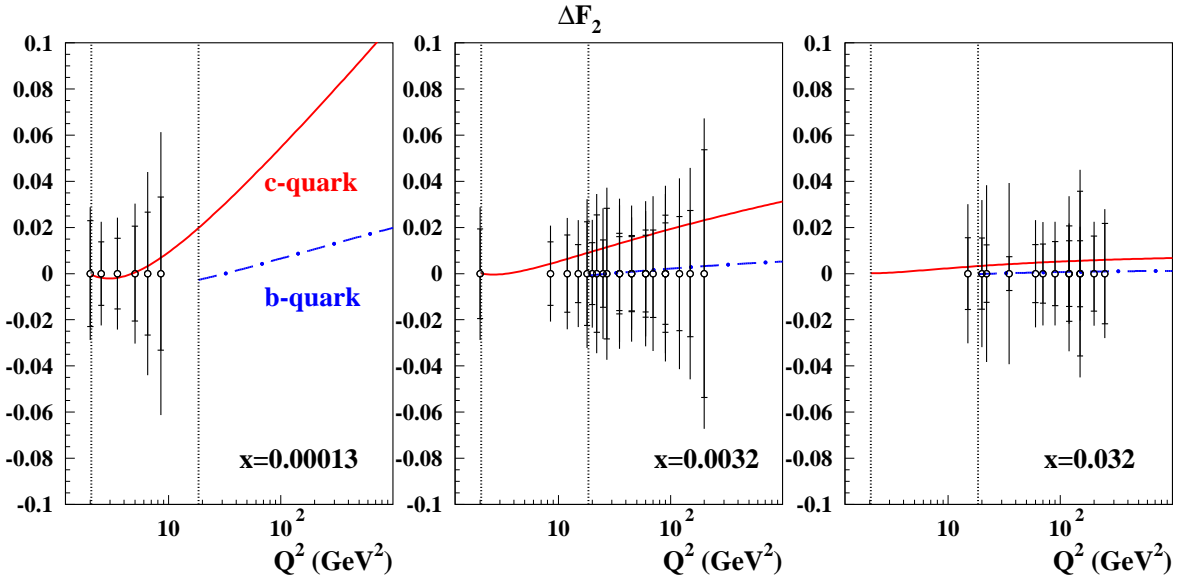


Figure 5: The errors in the inclusive structure function $F_2(x, Q^2)$ measured by the H1 collaboration [33] in comparison with the impact of the heavy quark scheme variation on the QCD calculations for $F_2(x, Q^2)$. Solid line: c -quark contribution, dash-dotted lines: b -quark contribution. The vertical dots mark the positions of $m_c = 1.43$ GeV and $m_b = 4.3$ GeV, respectively.

the asymptotic region is scaled to bigger values of Q^2 and the data are less precise due to the smaller scattering cross section. This is illustrated by a comparison of the ZEUS data on F_2^b with calculations of the 4-flavor ZMVFN scheme, the 3-flavor scheme, and the BMSN prescription for the GMVFN scheme given in Figure 4.

Also the inclusive structure function F_2 is sensitive to the choice of the heavy quark scheme, due to the significant charm contribution in the small x region. In fact, for F_2 the sensitivity is much larger than for the heavy quark contributions F_2^c and F_2^b alone due to the far higher accuracy of the data. In Figure 5 we compare the errors in F_2 measured by the H1 collaboration [33] with the difference between $F_2^{h,\text{exact}} - F_2^{h,\text{BMSN}}$. For b -quark production the scheme variation effect, which is calculated in the same way as in Figure 4, is negligible as compared to the accuracy of the data in the entire phase space. For the c -quark contributions, maximal sensitivity to the scheme choice appears at largest values of Q^2 at $x \sim 0.001$, similarly to the case of the data for F_2^c given in Figure 2. The effect is localized in phase space and appears to be at the margin of the statistical resolution. Therefore the impact of the scheme variation on the data analysis turns out to be rather mild. To check it in a more quantitative way we compare the QCD-analysis of the inclusive DIS data performed in the 3-flavor scheme with the one in the BMSN prescription of the GMVFN scheme. Details and results of these analyses are described in the following Section.

4 Impact of the Scheme Choice on the PDFs

We determine the PDFs from the inclusive DIS world data obtained at the HERA collider and in the fixed-target experiments [33, 34]. These data are supplemented by the fixed-target Drell-Yan data [35] and the di-muon data from (anti)neutrino-nucleon DIS [36], which allow the flavor separation of the sea quark distributions. Details of the data selection, the corrections applied to

	a	b	γ_1	γ_2	A
u_v	0.662 ± 0.034	3.574 ± 0.078	-0.590 ± 0.027	-0.71 ± 0.17	
d_v	1.06 ± 0.12	6.42 ± 0.41	4.4 ± 1.0	-7.0 ± 1.3	
u_s	-0.216 ± 0.011	6.83 ± 0.24	0.64 ± 0.29		0.1408 ± 0.0079
Δ	0.7	11.7 ± 1.9	-3.5 ± 2.1		0.256 ± 0.082
s	-0.253 ± 0.058	7.61 ± 0.65			0.080 ± 0.016
G	-0.214 ± 0.013	7.95 ± 0.15	0.65 ± 0.92		

Table 1: The parameters of the PDFs and their 1σ errors in the 3-flavor scheme.

the data, and statistical procedures used in the analysis can be found in Refs. [37, 38]. The analysis is performed taking into account the NNLO corrections for the light flavor contributions.

For the neutral-current c -quark contributions to the structure function F_2 two variants are compared, both up to the level of the $O(a_s^2)$ corrections.³ In one case we employ $F_2^{c,\text{exact}}(N_f = 3)$ of Eq. (1), calculated for three light quark flavors choosing the factorization scale of $\mu^2 = Q^2 + 4m_c^2$. This is compared to the BMSN prescription of the GMVFN scheme $F_2^{c,\text{BMSN}}(N_f = 4)$ given by Eq. (22) with the factorization scale $\mu^2 = Q^2$. However, in the kinematical region of the data this variation of scale yields no difference in the fit results. Our fit is based on the *reduced cross sections* rather than the DIS structure functions. Therefore we also have to consider the longitudinal structure function F_L . Since the data are much less sensitive to F_L than to F_2 the scheme choice is unimportant for the former and in both variants of the fit it is calculated in the $N_f = 3$ FFN scheme, Eq. (1). Likewise this is the case for the b -quark contribution, where the scheme choice is also unimportant, as one can see in the comparisons of Section 3. The $N_f = 3$ FFN scheme is used both for F_2^b and F_L^b . The charged-current c -quark contribution to the structure functions, which are related to the di-muon (anti)neutrino-nucleon DIS data used in the fit, are calculated in the $N_f = 3$ FFN scheme at NLO [39]. For the Drell-Yan cross sections, we include the NNLO QCD corrections [40]. In this case the 5-flavor PDFs defined in Eqs. (14–17) are used in order to take into account the c - and b -quark contributions. Note, however, that at the typical fixed-target energies the impact of heavy quarks is marginal and the 3-flavor scheme provides a sufficiently good description.

The proton PDFs are parameterized at the scale $Q_0^2 = 9 \text{ GeV}^2$ in the 3-flavor scheme. At the starting scale the following functions are used for the valence quark, gluon, and sea-quark

³The effects of the $O(a_s^3)$ corrections calculated recently in Ref. [8] will be studied in a forthcoming paper.

Table 2: Correlation matrix of the fitted parameters.

	a_u	b_u	$\gamma_{1,u}$	$\gamma_{2,u}$	a_d	b_d	A_d	b_Δ	A_u	a_{us}	b_{us}	a_G	b_G
a_u	1.0000	0.9256	0.9638	-0.2527	0.3382	0.2922	0.1143	-0.4267	0.4706	0.3117	0.1422	0.0982	0.1127
b_u		1.0000	0.9574	-0.5608	0.1933	0.1200	0.1058	-0.3666	0.3712	0.2674	0.1537	0.0453	0.1878
$\gamma_{1,u}$			1.0000	-0.4504	0.2328	0.2329	0.0906	-0.3379	0.4106	0.2876	0.0812	0.0491	0.1627
$\gamma_{2,u}$				1.0000	0.3007	0.3119	-0.0242	-0.0118	0.0587	0.0026	-0.0305	0.0949	-0.1876
a_d					1.0000	0.8349	-0.2010	-0.3371	0.3786	0.2592	0.1212	-0.0377	0.1305
b_d						1.0000	-0.2669	-0.0599	0.2768	0.1941	-0.0698	-0.0926	0.2088
A_d							1.0000	-0.2132	0.0549	0.0245	0.2498	-0.0523	0.0614
b_Δ								1.0000	-0.1308	-0.0729	-0.7208	-0.0124	-0.0225
A_u									1.0000	0.9240	-0.0723	0.3649	-0.1674
a_{us}										1.0000	-0.0144	0.2520	-0.1095
b_{us}											1.0000	-0.1274	0.1808
a_G												1.0000	-0.6477
b_G													1.0000

Table 2: continued.

	$\gamma_{1,G}$	$\alpha_s(3, 3 \text{ GeV})$	$\gamma_{1,\Delta}$	$\gamma_{1,us}$	$\gamma_{1,d}$	$\gamma_{2,d}$	A_s	b_s	a_s	a_Δ	m_c	m_b
a_u	-0.0727	-0.0611	0.3383	0.6154	0.2320	-0.0724	-0.0681	-0.0763	-0.0935	0.0026	0.0900	-0.0053
b_u	-0.1130	-0.1725	0.2992	0.4848	0.0849	0.0720	-0.0723	-0.0618	-0.0926	0.0049	0.0349	-0.0118
$\gamma_{1,u}$	-0.1106	-0.1338	0.2753	0.5638	0.1316	-0.0535	-0.0798	-0.0854	-0.1059	-0.0060	0.0817	0.0003
$\gamma_{2,u}$	0.1174	0.2195	-0.0210	0.0822	0.3712	-0.3310	0.0339	0.0143	0.0381	-0.0098	0.0430	-0.0004
a_d	-0.1631	-0.0208	0.0319	0.4974	0.9570	-0.4636	-0.0700	-0.0996	-0.0979	-0.2121	0.1066	-0.0150
b_d	-0.2198	-0.0913	-0.1775	0.4092	0.8985	-0.8498	-0.0533	-0.0669	-0.0806	-0.2252	0.0822	-0.0068
A_d	-0.0825	0.0188	0.8558	-0.0289	-0.2624	0.2852	-0.0075	-0.0189	-0.0180	0.9602	0.0420	0.0120
b_Δ	0.0530	-0.0801	-0.6666	-0.0904	-0.1981	-0.2532	-0.0022	0.0257	0.0048	-0.0260	-0.0166	-0.0056
A_u	0.2502	-0.0157	0.1265	0.7525	0.3047	-0.0668	-0.7064	-0.6670	-0.7267	0.0345	0.2137	0.0358
a_{us}	0.1845	-0.0216	0.0683	0.5714	0.2157	-0.0554	-0.8768	-0.8081	-0.8980	0.0145	0.0430	0.0074
b_{us}	-0.1619	-0.0715	0.5343	-0.3656	0.0293	0.2430	-0.0345	-0.0132	-0.0356	0.1527	-0.0899	-0.0058
a_G	0.8291	0.2306	-0.0260	0.3692	-0.0966	0.1496	0.0087	0.0007	0.0464	-0.0541	-0.0661	0.0417
b_G	-0.9184	-0.6145	0.0538	-0.2770	0.1990	-0.2552	0.0381	0.0616	-0.0468	0.0502	0.1847	0.0861

distributions :

$$xq_V(x, Q_0^2) = \frac{2\delta_{qu} + \delta_{qd}}{N_q^V} x^{a_q} (1-x)^{b_q} x^{P_{q,V}(x)}, \quad P_{q,V} = \gamma_{1,q}x + \gamma_{2,q}x^2, \quad q = u, d, \quad (23)$$

$$xG(x, Q_0^2) = A_G x^{a_G} (1-x)^{b_G} x^{P_G(x)}, \quad P_G = \gamma_{1,G}x, \quad (24)$$

$$xu_S(x, Q_0^2) = x\bar{u}_S(x, Q_0^2) = A_u x^{a_{us}} (1-x)^{b_{us}} x^{P_{u,S}(x)}, \quad P_{u,S} = \gamma_{1,us}x, \quad (25)$$

$$x\Delta(x, Q_0^2) = xd_S(x, Q_0^2) - xu_S(x, Q_0^2) = A_\Delta x^{a_\Delta} (1-x)^{b_\Delta} x^{P_\Delta(x)}, \quad P_\Delta = \gamma_{1,\Delta}x. \quad (26)$$

The strange quark distribution is taken in the charge-symmetric form

$$xs(x, Q_0^2) = x\bar{s}(x, Q_0^2) = A_s x^{a_s} (1-x)^{b_s}, \quad (27)$$

in agreement with the results of Ref. [38]. The polynomials $P(x)$ used in Eqs. (23–26) provide sufficient flexibility of the PDF-parameterization with respect to the analyzed data and no additional terms are required to improve the fit quality. The PDF-parameters determined from the fit performed in the 3-flavor scheme are given in Table 1. Because of the lack of the neutron-target data in the region of small values of x , the low- x exponent a_Δ cannot be defined from the fit and we fix it to 0.7 to choose an ansatz, in agreement with the values obtained for the low- x exponents of the valence quark distributions and phenomenological estimates, cf. e.g. [41]. However, once we have fixed a_Δ the uncertainty in the sea quark distributions at small x is underestimated. We therefore choose an uncertainty $\delta a_\Delta = 0.3$, and, in order to account for its impact on the other PDF-parameters, we calculate the errors in the latter with the value of a_Δ released, but with an additional pseudo-measurement of $a_\Delta = 0.7 \pm 0.3$ added to the data set. In our fit the heavy quark masses are fixed at $m_c = 1.5$ GeV and $m_b = 4.5$ GeV and the same approach is employed to take into account possible variations of m_c and m_b in the ranges of ± 0.1 GeV and ± 0.5 GeV, respectively. Note that the normalization parameters for the valence quarks and gluons are defined from other PDF-parameters applying both fermion number- and momentum conservation. In the global fit we obtain

$$\frac{\chi^2}{\text{NDP}} = \frac{3038}{2716} = 1.1 \quad (28)$$

for the parameter values listed in Table 1.

In the fit 25 parameters are determined. The covariance matrix elements for these parameters are given in Table 2. The parameter errors quoted are due to the propagation of the statistical and systematic errors in the data. The error correlations are taken into account if available, which is the case for most of the data sets considered.

The gluon and flavor singlet distributions obtained in case of the BMSN prescription are compared to those referring to the 3-flavor scheme in Figure 6. The difference between the two variants is quite small and situated well within the PDF-uncertainties. For the non-singlet PDFs it is even smaller, since the heavy quark contribution is negligible at $x \gtrsim 0.1$, cf. Ref. [42]. For the BMSN variant of the fit a value of $\chi^2/\text{NDP} = 3036/2716$ is obtained, very close to the one for the fit in the 3-flavor scheme. This is in line with the comparisons given in Section 3, which show that in the case of a smooth matching of the 3-flavor and VFN scheme at small values of Q^2 , there is little room for a difference between them in the region of the present experiments.

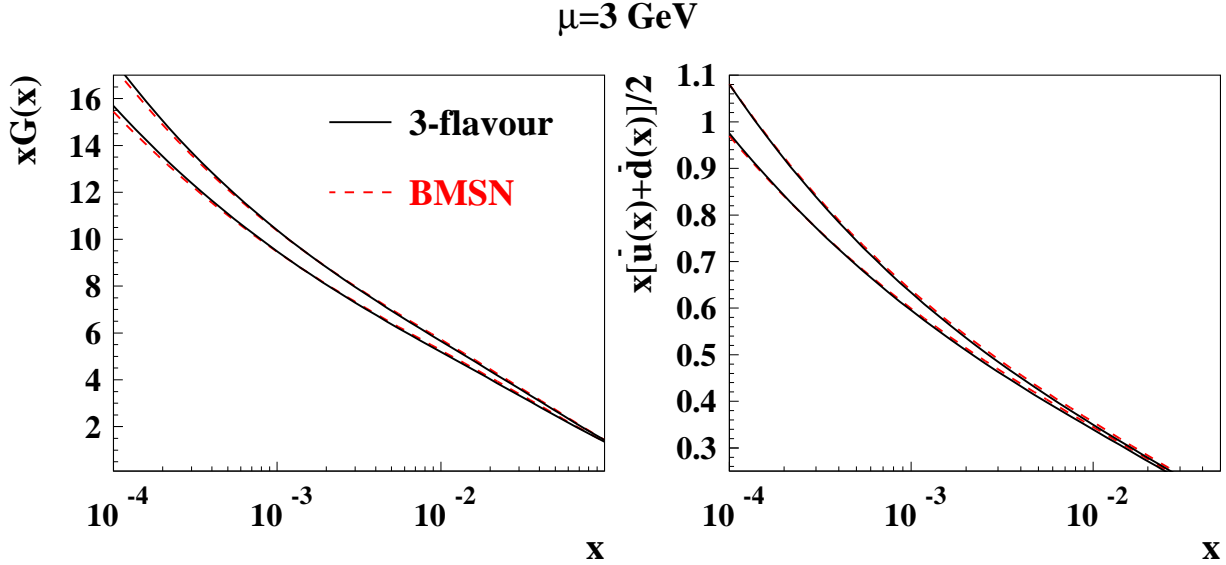


Figure 6: The 1σ error band for the gluon (left panel) and sea (right panel) distributions obtained in two variants of the fit. Solid lines: 3-flavour scheme, dashed lines : GMVFN scheme in the BMSN prescription.

The difference between the fits performed using the TR-prescription for the GMVFN scheme and in the 3-flavor scheme is also not dramatic, as one can see in the ZEUS NLO PDF fit, Ref. [43]. However, it is somewhat larger than in the case of the BMSN prescription. In particular, this happens since the TR-prescription does not provide a smooth matching with the 3-flavor scheme at low values of Q^2 and at small values of x . By construction, the TR-prescription provides a smooth transition for the *gluon-initiated* contribution only. However, at small values of Q^2 the gluon distribution has a valence-like form and falls at small x . As a result, the quark-singlet contribution to the slope $\partial F_2^c / \partial \ln(Q^2)$ is non-negligible at small values of x , which leads to a kink at the matching point $Q^2 = m_h^2$ in F_2^h using the TR-prescription, see Figure 7. This is an artefact of the description leading to an overestimation of the heavy quark contribution and, correspondingly, an underestimation of the fitted light quark PDFs at small values of x . In the ACOT(χ)-prescription the smoothness is not required by definition and the kink in F_2^h is even bigger than for the case of TR-prescription. In the most recent version of the ACOT-prescription this problem is addressed [44] and should yield a result closer to the 3-flavor scheme than the ACOT(χ)-prescription.

Summarizing the comparisons of Sections 3 and 4 we conclude that, once the $O(\alpha_s^2)$ corrections to heavy quark electro-production are taken into account and a smooth matching with the 3-flavor scheme at small Q^2 is provided, the GMVFN scheme should agree to the 3-flavor scheme for the kinematics explored by experiments so far. Furthermore, it is expected that the NNLO corrections to the heavy quark structure functions of Ref. [8] lead to an even better agreement.

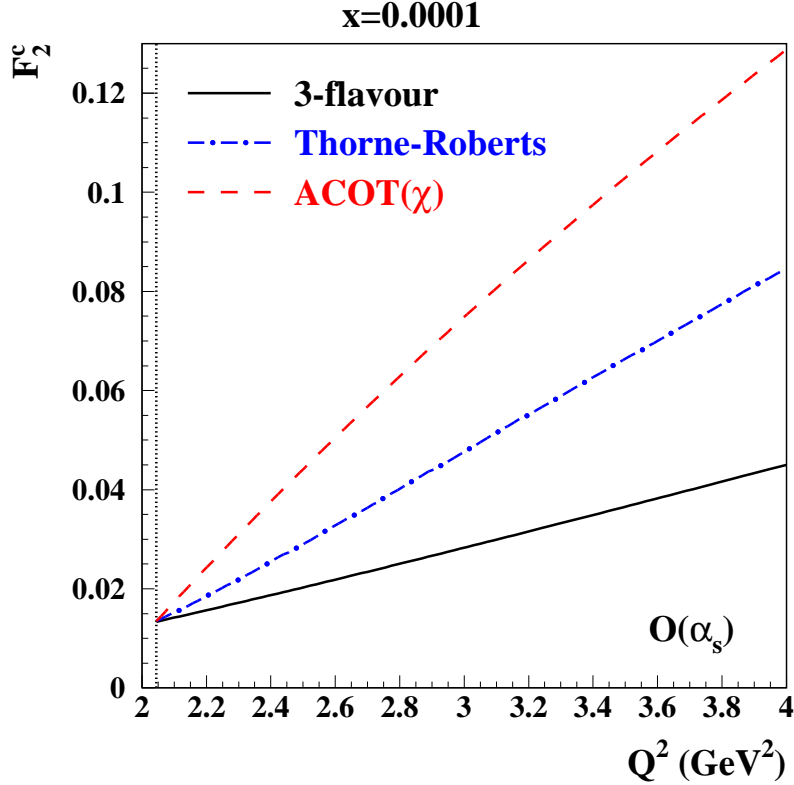


Figure 7: Matching of $F_2^{c,\text{TR}}(x, Q^2)$ (dash-dotted line) and $F_2^{c,\text{ACOT}(\chi)}(x, Q^2)$ (dashed line) with $F_2^{c,\text{exact}}(N_f = 3, x, Q^2)$ (solid line) at small Q^2 at $O(\alpha_s)$. The MRST2001 PDFs of Ref. [29] are used. The vertical line denotes the position of the charm-quark mass $m_c = 1.43$ GeV.

For the strong coupling constant at NNLO in QCD the values

$$\alpha_s^{\overline{\text{MS}}}(N_f = 5, M_Z^2) = 0.1135 \pm 0.0014 \text{ (exp)} \quad \text{FFN scheme, } N_f = 3 \quad (29)$$

$$\alpha_s^{\overline{\text{MS}}}(N_f = 5, M_Z^2) = 0.1129 \pm 0.0014 \text{ (exp)} \quad \text{BMSNscheme} \quad (30)$$

are obtained. The small difference between these two values lies well within the experimental uncertainty. In Table 3 we compare these values to other recent NNLO determinations of the strong coupling constant. Our results agree very well with those of Refs. [42, 45]. Note that the data sets used in the non-singlet fit of Ref. [42] are rather different from those used in the present analysis. The value of $\alpha_s(M_Z^2)$ given in Ref. [46] is by 2.7σ larger. As is well-known from the non-singlet data analysis [42], a somewhat higher value of $\alpha_s(M_Z^2)$ is obtained at N³LO, cf. also Ref. [21] for an estimate. The difference of these determinations at NNLO and N³LO is half of the experimental error found in the present analysis. Eqs. (29) and (30) determine $\alpha_s(M_Z^2)$ at an accuracy of $\approx 1.5\%$.

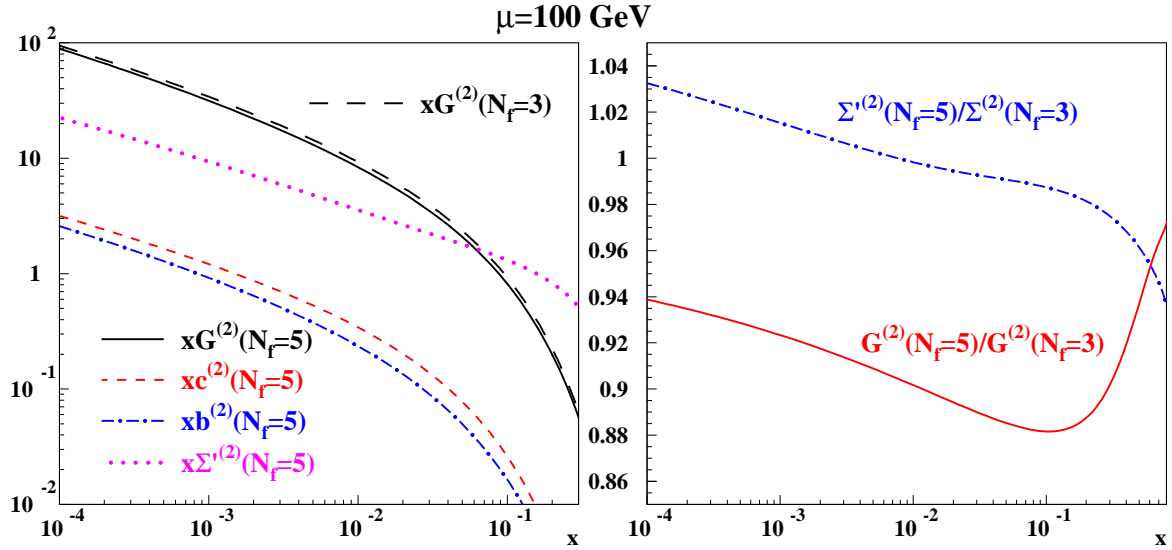


Figure 8: Left panel: The 5-flavor PDFs at the scale of $\mu^2 = 10^4 \text{ GeV}^2$ and the 3-flavor gluon distribution given for comparison. Right panel: The ratio of the 5-flavor to 3-flavor gluon (solid line) and singlet (dash-dotted line) distributions at the same scale.

5 Applications to Collider Phenomenology

In this Section, we investigate the implications of the PDFs obtained in the present NNLO analysis for collider phenomenology. To that end we focus on important (semi)-inclusive scattering cross sections at hadron colliders, such as the Drell-Yan process for W^\pm - and Z -boson production, the pair-production of top-quarks and (Standard Model) Higgs-boson production. The corresponding cross sections in, say, proton-proton scattering can be written as

$$\sigma_{pp \rightarrow X}(s) = \sum_{ij} \int dx_1 dx_2 f_i(x_1, \mu^2) f_j(x_2, \mu^2) \hat{\sigma}_{ij \rightarrow X}(x_1, x_2, s, \alpha_s(\mu^2), \mu^2), \quad (31)$$

where X is the final state under consideration and s the c.m.s. energy. The PDFs are collectively denoted by f_i , f_j and the sum runs over all partons. At hadron colliders the convolution of f_i and f_j parameterizes the so-called parton luminosity L_{ij} . In the following, we will employ our PDFs and present numbers for $p\bar{p}$ -collisions at Tevatron with $\sqrt{s} = 1.96 \text{ TeV}$ and for pp -collisions at LHC at energies $\sqrt{s} = 7, 10$ and 14 TeV . To that end, we have to rely on the perturbative QCD evolution of the light and heavy PDFs to Tevatron and LHC scales, which puts us also in the position to compare to other global PDF analyses. In the comparison we will consider the impact of the error of the PDFs at the level $1\sigma_P$ (the index P denoting PDFs), which results from the experimental errors in the PDF analysis, including full error correlation, see Section 4. We will not consider theory errors implied by varying the factorization and renormalization scales. At the level of NNLO these amount typically to a few per cent only and, moreover, are largely independent of

	$\alpha_s(M_Z^2)$	
ABKM	0.1135 ± 0.0014	heavy quarks: FFN $N_f = 3$
ABKM	0.1129 ± 0.0014	heavy quarks: BMSN approach
BBG [42]	$0.1134^{+0.0019}_{-0.0021}$	valence analysis, NNLO
AMP06 [37]	0.1128 ± 0.0015	
JR [45]	0.1124 ± 0.0020	dynamical approach
MSTW [46]	0.1171 ± 0.0014	
BBG [42]	$0.1141^{+0.0020}_{-0.0022}$	valence analysis, N ³ LO

Table 3: Comparison of different measurements of $\alpha_s(M_Z^2)$ at NNLO and higher order.

the PDFs. Also the anticipated statistical and systematic errors in the measurements at Tevatron and the corresponding resolutions, which can be achieved at the LHC, are not considered.

5.1 Evolution of Light and Heavy PDFs

The typical energy scales for hard scattering processes at high-energy hadron colliders are often much larger than the c -quark mass, and even than the b -quark mass. In this case the (4–)5–flavor scheme is the relevant choice, if power corrections and non-factorizing contributions can be safely neglected. Moreover, very often this is the only approach feasible, since the cross sections of the partonic sub-processes are only available in the approximation of massless initial-state partons. The 3-flavor PDFs obtained from the fit in Section 4 can be used to generate the 4-flavor distributions using the matching conditions in Eqs. (14–17). As we show in Figure 3, at $O(\alpha_s^2)$ and low scales, the PDFs computed in this way are very similar to the evolved ones, provided the matched PDFs are taken as boundary conditions in the evolution. At large scales the difference between these two cases is non-negligible, contrary to the case of heavy quark DIS electro-production. The large-log resummation effects can be important in some range of the phase space at hadron colliders. In view of these aspects we obtain the 4-flavor PDFs from the NNLO evolution with the boundary scale m_c^2 and the boundary conditions given in Eqs. (14–17). The 5–flavor PDFs are obtained from the evolved 4-flavor distributions using analogous boundary conditions at the scale m_b^2 . Since at m_b^2 the mass effects of the charm-quark are not negligible due to $m_b^2/m_c^2 \sim 10$, this approach is *some approximation*, the validity of which has to be tested for the corresponding processes. The problem of the heavy quark mass scale separation cannot be resolved within the concept of a VFN scheme and implies an unavoidable theoretical uncertainty related to the use of VFN PDFs. In general, the heavy quark PDFs rise with the scale μ^2 , while the $(N_f + 1)$ -light PDFs decrease correspondingly with respect to N_f -light PDFs. At the scale of 10^4 GeV^2 the 5-flavor gluons lose some 7% of momentum as compared to the 3-flavor ones. This momentum is transferred to the c - and b -quark distributions, see Figure 8. The difference between the 3-flavor

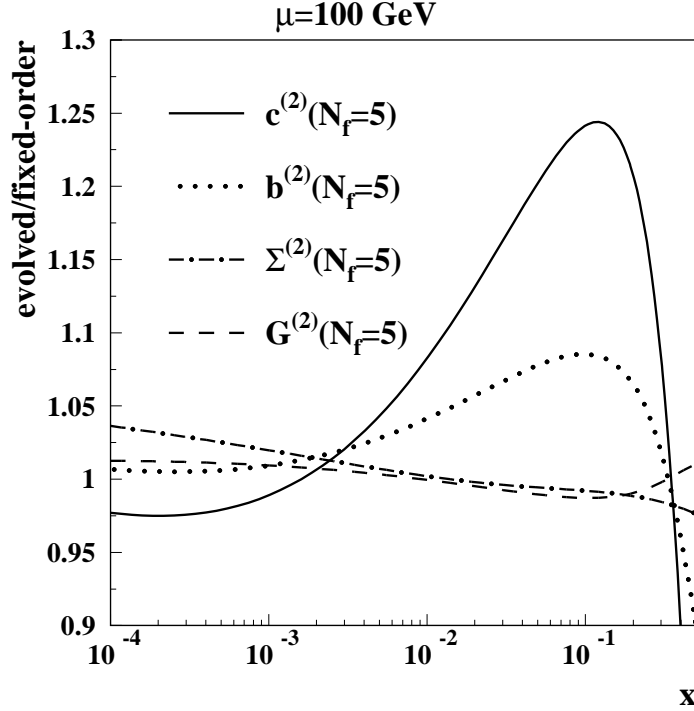


Figure 9: Ratio of the evolved NNLO 5-flavor distributions to the distributions being obtained applying the fixed-order matching conditions of Eqs. (14–17).

singlet distribution $\Sigma(N_f = 3)$ and the 5-flavor distribution

$$\Sigma'(N_f = 5) = \sum_{k=1}^3 [q_k(N_f = 5) + \bar{q}_k(N_f = 5)] \quad (32)$$

is smaller than that for the gluons since in the quark-case the corresponding OMEs appear only at $O(\alpha_s^2)$. At small values of x the 5-flavor light quark and gluon distributions receive an additional enhancement as compared to the 3-flavor distributions due to evolution, see Figure 9. This difference can be considered as an estimate of the theoretical uncertainty in the 5-flavor PDFs due to the higher order corrections. For the c - and b -quark distributions at $x \sim 0.1$ the effect of the evolution is much larger. However, due to the smallness of the heavy quark PDFs in this region its absolute magnitude is insignificant for most practical purposes.

5.2 Comparison with Other NNLO Analyses

In Figures 10 and 11 we compare the NNLO PDFs obtained in the present analysis to the PDFs by Martin-Stirling-Thorne-Watt of 2008 (MSTW 2008), [47]. At the scales of $\mu^2 = 100 \text{ GeV}^2$ and $\mu^2 = 10^4 \text{ GeV}^2$, we compare the 5-flavor PDFs and at the scale of $\mu^2 = 4 \text{ GeV}^2$, the 4-flavor PDFs since for the MSTW2008 set the number of flavors is four at $m_c < \mu < m_b$ and 5 at $\mu > m_b$ ⁴. At small

⁴If the scale is not much larger than m_c^2 the choice of 3-flavor PDFs is most relevant, cf. Sections 2,3.

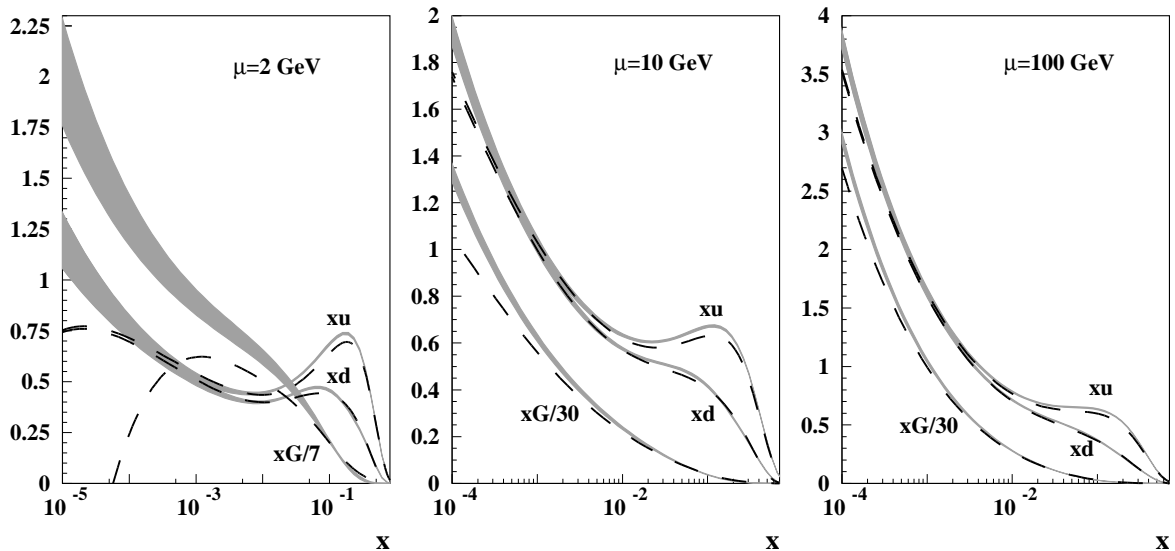


Figure 10: The 1σ error bands (shaded area) for our NNLO 4-flavor (left panel) and 5-flavor (central and right panels) u -, d -quark, and gluon distributions in comparison to the corresponding MSTW2008 NNLO distributions [47] (dashed lines).

values of x our gluon distribution is larger than that of MSTW2008. This difference is particularly essential at smaller scales where the NNLO MSTW2008 gluon distribution becomes negative at $x \sim 5 \cdot 10^{-5}$. This is not the case in our analysis. Also our sea-quark distributions are larger than those of MSTW2008 in the small- x region. As we discuss in Section 4, this might be partly related to the heavy quark contribution in the GMVFN scheme employed in the MSTW2008 fit. The shape of the gluon distribution at small x is sensitive to the recent measurements of F_L at small Q^2 by the H1 and ZEUS collaborations [48]. These measurements are in agreement with our shape for the gluon and do slightly disfavor the MSTW2008 predictions. At large x the MSTW2008 gluon distribution is somewhat larger than ours due to the impact of the Tevatron jet data included in the MSTW2008 analysis.

In Figure 12 we compare our 3-flavor PDFs to the results obtained by the Dortmund group [Jimenes-Delgado and Reya (JR)] in Ref. [45], for $\mu^2 = 4, 100$ and 10000 GeV^2 . At $\mu^2 = 4 \text{ GeV}^2$ the gluon PDF [45] is somewhat smaller for $x \lesssim 5 \cdot 10^{-5}$ than the gluon distribution determined in the present fit. This is a region in which the fit is not constrained by data. A very small difference is also observed for the u - and d -quark distributions in the region $x \sim 0.1$. Otherwise, one notices very good agreement of both distributions.

In Table 4 we summarize different values of the 2nd moment of the valence quark densities.⁶

⁵We thank P. Jimenez-Delgado and W.J. Stirling for providing us with the moments of the JR and MSTW08 distributions.

⁶Here and in the following we restrict the comparison to the results obtained in NNLO analyses. Currently available NLO analyses (see in Ref. [42] and Refs. [33, 49–51]) contain relatively large theory uncertainties of ± 0.0050 for

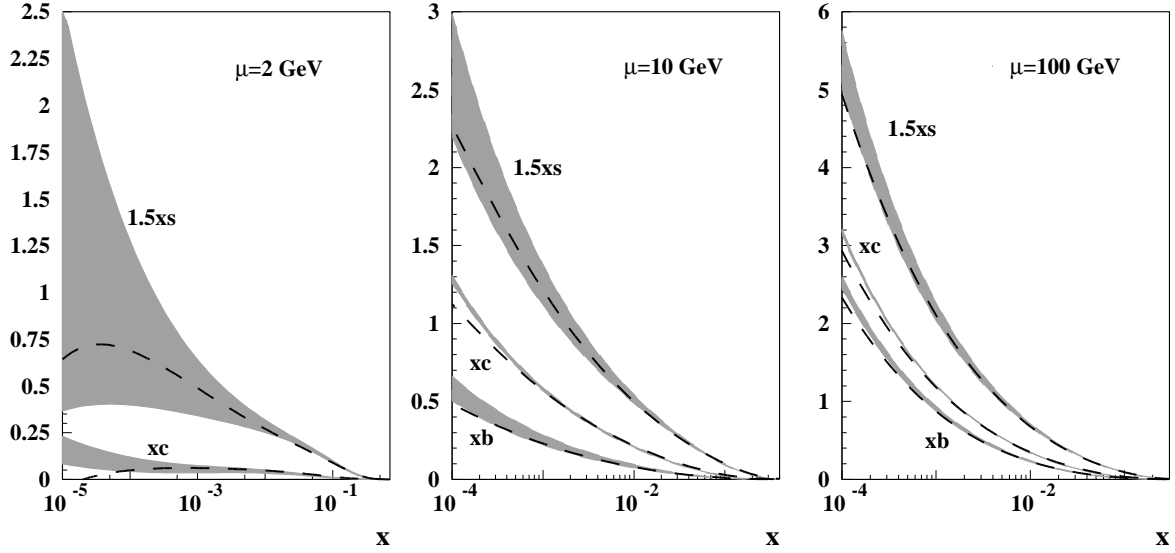


Figure 11: The 1σ error bands (shaded area) for our NNLO 4-flavor (left panel) and 5-flavor (central and right panels) s -, c -, and b -quark distributions in comparison to the corresponding MSTW2008 NNLO distributions [47] (dashed lines).

They are closely related to the moments which are currently measured in lattice simulations [52]. The values of all analyses are very similar, with some differences still visible. A quantity of central importance is

$$\langle xV(Q^2) \rangle = \int_0^1 dx x \{ [u(x, Q^2) + \bar{u}(x, Q^2)] - [d(x, Q^2) + \bar{d}(x, Q^2)] \}. \quad (33)$$

In the present analysis we obtain

$$\langle xV(Q_0^2) \rangle = 0.1646 \pm 0.0027 \quad (\text{this analysis}) \quad (34)$$

$$\langle xV(Q_0^2) \rangle = 0.1610 \pm 0.0043 \quad \text{N}^3\text{LO}, \quad (35)$$

for $Q_0^2 = 4 \text{ GeV}^2$, where we combine in Eq. (35) the value of the difference $x(u_v - d_v)$ obtained in Ref. [42] with the value for

$$\langle x[\bar{d} - \bar{u}] \rangle = 0.0072 \pm 0.0007 \quad (36)$$

found in the present analysis. In the above combination the correlation to the heavier flavor distributions is negligible.

The PDF-uncertainties given in Figures 10-12 are defined by the uncertainties in the analyzed data and the uncertainties due to m_c , m_b , and the low- x non-singlet exponent a_Δ as discussed in Section 4. For the c - and b -quark distributions, the essential uncertainties are due to m_c and m_b ,

$\alpha_s(M_Z^2)$, much larger than the experimental accuracy presently reached.

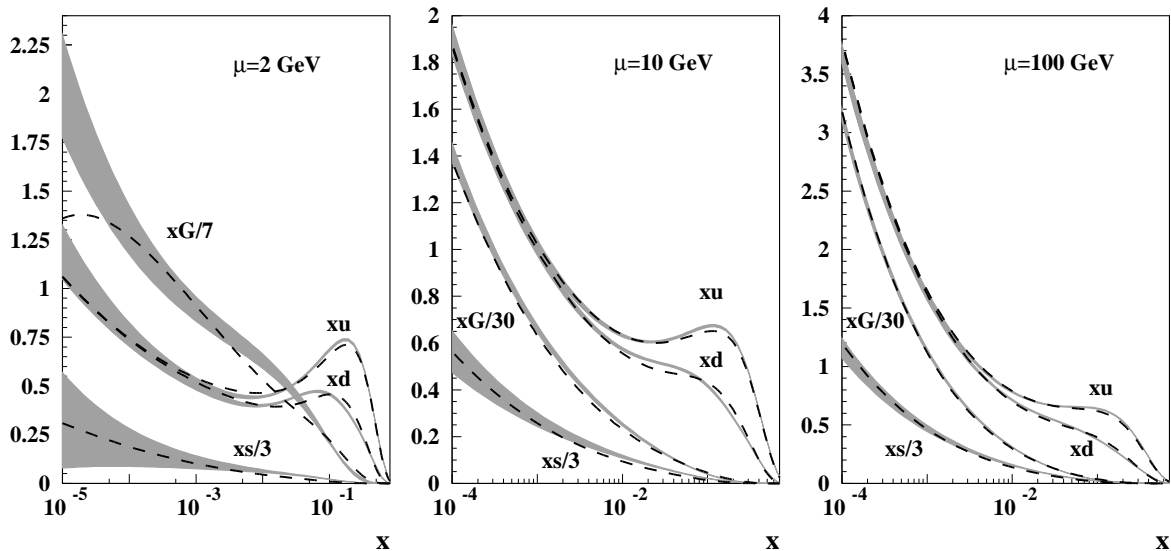


Figure 12: The 1σ error bands (shaded area) for our NNLO 3-flavor u -, d -, s -quark and gluon distributions in comparison to the corresponding JR NNLO distributions [45] (dashed lines).

respectively. At small x , however they are determined much more precisely than the strange sea distribution, which is widely unconstrained at $x \lesssim 0.01$ by the present data. We now turn to some important inclusive processes at hadron colliders, for which we illustrate the impact of NNLO PDFs derived in the present analysis.

5.3 W/Z -boson Production

The inclusive production cross sections of single W^\pm - and Z -bosons are considered so-called standard candle processes at hadron colliders. The cross sections and distributions for these processes are calculated up to the NNLO [40, 53–55] (see also Ref. [56] for the expressions in Mellin-space) which allows to reduce the theoretical uncertainty due to factorization and renormalization scale variation down to a few per cent. With this theoretical accuracy provided the measurement of the W^\pm/Z -boson production rates can be used to monitor the luminosity of the collider. Moreover, a combination of the data on W^\pm/Z -production with the non-resonant Drell-Yan data allows to separate the quark distributions of different flavors with a very good accuracy, cf. [57]. The quark-anti-quark luminosities contributing to W^+ -production in pp collisions are given by

$$L_{q\bar{q}} = \tau \left[q(\sqrt{\tau}e^Y, M_W)\bar{q}(\sqrt{\tau}e^{-Y}, M_W) + \bar{q}(\sqrt{\tau}e^Y, M_W)q(\sqrt{\tau}e^{-Y}, M_W) \right], \quad (37)$$

where $\tau = M_W^2/s$, s denotes the c.m.s. collision energy squared, and Y is the W^+ c.m.s rapidity. In Figure 13 we compare the luminosities of Eq. (37) weighted by the corresponding Cabibbo-Kobayashi-Maskawa (CKM) matrix elements $V_{q_i\bar{q}_j}^2$ for different channels at the energy of the LHC with our NNLO 5-flavor PDFs used as input and

	$\langle xu_v(x) \rangle$	$\langle xd_v(x) \rangle$	$\langle x[u_v - d_v](x) \rangle$
ABMK	0.2981 ± 0.0025	0.1191 ± 0.0023	0.1790 ± 0.0023
BBG [42]	0.2986 ± 0.0029	0.1239 ± 0.0026	0.1747 ± 0.0039
JR [45]	0.2900 ± 0.0030	0.1250 ± 0.0050	0.1640 ± 0.0060
MSTW [46]	$0.2816^{+0.0051}_{-0.0042}$	$0.1171^{+0.0027}_{-0.0028}$	$0.1645^{+0.0046}_{-0.0034}$
AMP06 [37]	0.2947 ± 0.0030	0.1129 ± 0.0031	0.1820 ± 0.0056
BBG [N ³ LO] [42]	0.3006 ± 0.0031	0.1252 ± 0.0027	0.1754 ± 0.0041

Table 4: Comparison of the 2nd moment of the valence quark distributions at NNLO and N³LO obtained in different analyses at $Q^2 = 4 \text{ GeV}^2$.⁵

\sqrt{s} [TeV]	this paper		MSTW [47]	
	$\sigma(W^+ + W^-)$	$\sigma(Z)$	$\sigma(W^+ + W^-)$	$\sigma(Z)$
1.96 ($\bar{p}p$)	26.2 ± 0.3	7.73 ± 0.08	25.4 ± 0.4	7.45 ± 0.13
7 (pp)	98.8 ± 1.5	28.6 ± 0.5		
10 (pp)	145.6 ± 2.4	42.7 ± 0.7	142.1 ± 2.4	42.5 ± 0.7
14 (pp)	207.4 ± 3.7	61.4 ± 1.1	201.1 ± 3.3	61.0 ± 1.0

Table 5: The total W^\pm and Z -cross sections [nb] at the Tevatron and LHC at the scale $\mu = M_{W/Z}$ (see Eq. (38) for the other parameters) with the PDFs and its estimated uncertainties from the present analysis and in comparison to results of Ref. [47].

$$V_{u\bar{d}}^2 = V_{c\bar{s}}^2 = 0.9474, \quad V_{u\bar{s}}^2 = 0.0509, \quad M_W = 80.398 \text{ GeV} . \quad (38)$$

In the forward region of rapidity the main contribution comes from the $u\bar{d}$ annihilation. In the central region the c -quark contribution is also essential. Therefore, the single W^\pm cross section measurement can be used to check the magnitude of the c -quark distribution. For the case of antiproton-proton collisions, the quark-anti-quark luminosities are similar to Eq. (37); however, at Tevatron the valence u -quark contribution is dominating in the whole range of rapidity. The cross sections for W^\pm/Z -production at the scale $\mu = M_{W/Z}$ for the parameters in Eq. (38), and $M_Z = 91.188 \text{ GeV}$, and including the NNLO corrections of Refs. [53,54] are given in Table 5. The quoted uncertainties are propagated from the uncertainties in the parameters of our PDFs, α_s , m_c and m_b , cf. Section 4. They amount to $\sim 1\%$ at the Tevatron and $\sim 2\%$ at the LHC. Comparing the present analysis to Ref. [47] the results for Tevatron are at variance by $2\sigma_P$, while the same cross sections are obtained for Z -boson production at LHC energies.

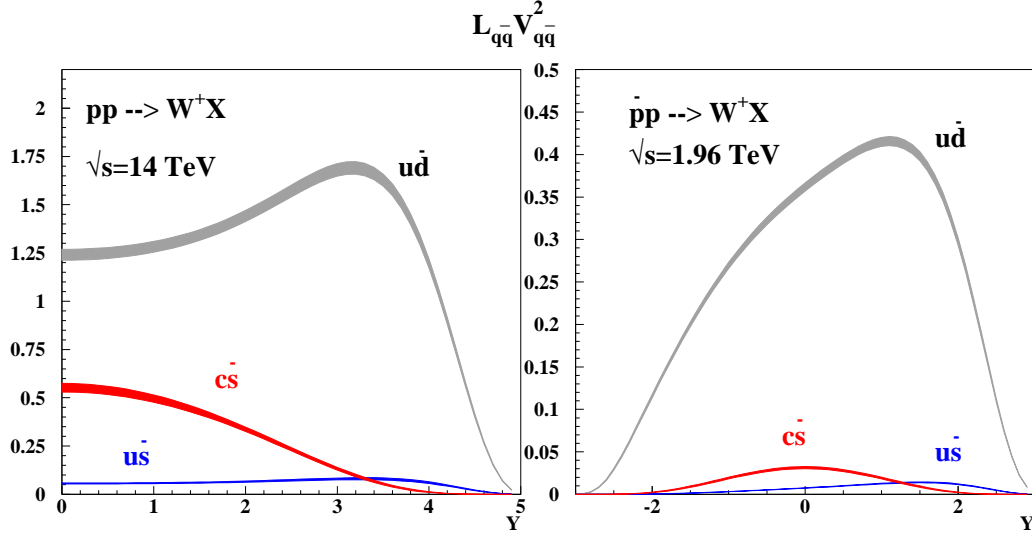


Figure 13: The 1σ band for the quark-anti-quark luminosities contributing to the W^+ production in the proton-proton collisions at the c.m.s. energy of $\sqrt{s} = 14$ TeV (left panel) and antiproton-proton collisions at the c.m.s. energy of $\sqrt{s} = 1.96$ TeV (right panel).

5.4 Top-quark Pair-Production

The scattering cross section for hadroproduction of heavy quarks of mass m_h is known exactly in QCD including radiative corrections at NLO [58–61]. At NNLO approximate results based on the complete logarithmic dependence on the heavy quark velocity $\beta = \sqrt{1 - 4m_h^2/\hat{s}}$ near threshold $\hat{s} \approx 4m_h^2$ (\hat{s} being the partonic c.m.s. energy) together with the exact dependence on the scale μ provide currently the best estimates [62, 63]. At Tevatron, the cross section is most sensitive to the $q\bar{q}$ -

\sqrt{s} (TeV)	this paper	MSTW2008
1.96 ($\bar{p}p$)	6.91 ± 0.17	7.04
7 (pp)	131.3 ± 7.5	160.5
10 (pp)	343 ± 15	403
14 (pp)	780 ± 28	887

Table 6: The total $t\bar{t}$ -production cross sections [pb] at the Tevatron and LHC for a pole mass of $m_t = 173$ GeV at the scale $\mu = m_t$. The results for the PDFs and its estimated uncertainties from the present analysis are compared to the central values obtained using the PDFs of Ref. [47].

annihilation channel, with the luminosities L_{ij} ordered in magnitude according to $L_{q\bar{q}} > L_{qg} > L_{gg}$. At the LHC, on the other hand, the cross section receives the dominant contribution from the gg -channel, in particular, from the gluon PDF in the region $x \approx 2.5 \cdot 10^{-2}$. This makes the cross section for top-quark pair-production an interesting observable to investigate the gluon luminosity. Also the correlations of rates for $t\bar{t}$ -pairs with other cross sections can be studied quantitatively [64].

Our cross sections for $t\bar{t}$ -production are summarized in Table 6 for a pole mass of $m_t = 173$ GeV. We estimate the relative accuracy due to the PDF-fit for Tevatron by $\sim 3\%$, and for the LHC by $\sim 3.5 - 4.5\%$. With comparison of the cross sections obtained with the PDFs of Ref. [47] we find agreement within $1\sigma_P$ for Tevatron. For LHC energies, the results for the MSTW08 set are larger by $4\sigma_P$ due to a bigger value of $\alpha_s(M_Z^2)$ and the larger value of the gluon PDF in the partonic threshold region $\hat{s} \simeq 4m_t^2$. Note that the variation of the factorization and renormalization scale is not considered here. It contributes separately to theoretical uncertainty (at NNLO $\sim 3 - 4\%$ at Tevatron and LHC, see [62, 63] for details).

5.5 Higgs Boson Production

Higgs-boson production is the most prominent signal at LHC and currently subject to intensive searches at Tevatron. The gluon-fusion channel (via a top-quark loop) is by far the largest production mode and known including the NNLO QCD corrections [54, 65–67].

In Table 7 the total production cross sections for the Higgs-boson are presented as a function of the Higgs-boson mass m_H at Tevatron and for a series of foreseen collision energies at the LHC (using $m_t = 173$ GeV). The relative error from the PDF fit amounts to $5.5 - 10\%$ at Tevatron and to $2.5 - 3\%$ at the LHC at the higher energies and to $3.5 - 4.5\%$ at $\sqrt{s} = 7$ TeV. Again we do not consider the theoretical uncertainty due to the variation of the factorization and renormalization scale (typically amounting to $\sim 9 - 10\%$ at NNLO). In Figure 14 we compare the production cross sections to the results obtained using the PDFs of Ref. [47]. The MSTW08 predictions yield higher values. For the LHC energies both analyses agree at lower Higgs masses $M_H \sim 100$ GeV and a gradual deviation reaching $3\sigma_P$ at $M_H = 300$ GeV of the MSTW08 values is observed. Our values at Tevatron are lower than those of MSTW08 by $\sim 3\sigma_P$ in the whole mass range. At the LHC energies the difference can be attributed to different gluon PDFs and values for α_s . The cross sections take very similar values for light Higgs masses, but beyond scales $\mu^2 \sim 10^4$ GeV² the values obtained with MSTW08 are larger.

6 Conclusions

The precision of the DIS world data has reached a level which requires NNLO analyses to determine the PDFs and to measure the strong coupling constant $\alpha_s(M_Z^2)$. This also applies to the most prominent scattering processes at hadron colliders such as the Drell-Yan process, W^\pm -, Z-boson, Higgs-boson and top-quark pair-production. In the present analysis we have performed an NNLO fit to the DIS world data, Drell-Yan- and di-muon data along with a careful study of the heavy flavor effects in the DIS structure function F_2 . In the analysis we have taken into account correlated errors whenever available. In total, 25 parameters have been fitted yielding a positive semi-definite covariance matrix. With this information one may predict the error with respect to the PDFs, $\alpha_s(M_Z^2)$, m_b and m_c for hard cross sections measured, including all correlations. For applications to hadron collider processes we have determined 3-, 4- and 5-flavor PDFs within the

m_H/GeV	Tevatron	LHC 7 TeV	LHC 10 TeV	LHC 14 TeV
100.	1.381 ± 0.075	21.19 ± 0.58	39.17 ± 1.05	67.28 ± 1.77
110.	1.022 ± 0.061	17.30 ± 0.49	32.52 ± 0.88	56.59 ± 1.51
120.	0.770 ± 0.049	14.34 ± 0.41	27.38 ± 0.72	48.25 ± 1.23
130.	0.589 ± 0.041	12.03 ± 0.36	23.33 ± 0.61	41.60 ± 1.07
140.	0.456 ± 0.033	10.21 ± 0.31	20.08 ± 0.55	36.23 ± 0.92
150.	0.358 ± 0.028	8.75 ± 0.27	17.45 ± 0.48	31.83 ± 0.82
160.	0.283 ± 0.024	7.56 ± 0.24	15.29 ± 0.43	28.20 ± 0.72
170.	0.226 ± 0.020	6.59 ± 0.21	13.51 ± 0.37	25.16 ± 0.65
180.	0.183 ± 0.017	5.78 ± 0.19	12.01 ± 0.35	22.60 ± 0.60
190.	0.148 ± 0.014	5.11 ± 0.17	10.75 ± 0.31	20.44 ± 0.53
200.	0.121 ± 0.013	4.55 ± 0.16	9.69 ± 0.28	18.59 ± 0.49
210.		4.07 ± 0.15	8.78 ± 0.26	17.01 ± 0.44
220.		3.67 ± 0.14	8.00 ± 0.24	15.64 ± 0.42
230.		3.32 ± 0.13	7.33 ± 0.22	14.46 ± 0.38
240.		3.02 ± 0.12	6.75 ± 0.21	13.44 ± 0.37
250.		2.77 ± 0.11	6.25 ± 0.20	12.55 ± 0.35
260.		2.55 ± 0.10	5.82 ± 0.19	11.79 ± 0.32
270.		2.36 ± 0.10	5.45 ± 0.18	11.12 ± 0.31
280.		2.19 ± 0.10	5.13 ± 0.17	10.56 ± 0.30
290.		2.06 ± 0.09	4.86 ± 0.17	10.08 ± 0.29
300.		1.94 ± 0.09	4.63 ± 0.16	9.69 ± 0.28

Table 7: The total cross sections for Higgs-boson production [pb] at Tevatron and the LHC at the scale $\mu = M_H$ with the uncertainties estimated from the fit results in the present analysis.

GMVFN scheme applying the BMSN description. We have performed a detailed study of the heavy flavor contributions to deep inelastic scattering comparing to experimental data. We have compared to different treatments used in the literature and found that both the FFN scheme and the BMSN scheme yield a concise description of the DIS data at least for the kinematic range of HERA, and that no modifications of these renormalization group-invariant prescriptions are needed. In the present analysis we have obtained $\alpha_s(M_Z^2)$ with an accuracy of $\approx 1.5\%$. The values quoted in Eqs. (29) and (30) are found to be in very good agreement with the non-singlet analysis of Ref. [42], which relied on a sub-set of the present data only, and with the results of Ref. [45]. The central value of $\alpha_s(M_Z^2)$ steadily converges going from LO to NLO to NNLO, or even to N³LO in the non-singlet case [42]. The differences in the central values (determined at $\mu^2 = Q^2$) provide a good estimate of the remaining theory errors. It is very hard to achieve a better accuracy on $\alpha_s(M_Z^2)$ than obtained at the moment, given the theoretical uncertainties (reaching values around $\sim 0.7\%$), which arise from the difference between the FFN and BMSN scheme, from quark mass effects, from 4-loop effects in the strong coupling constant from (the yet unknown) effect of the 4-loop singlet anomalous dimensions, or from remainder higher twist effects and so on. However,

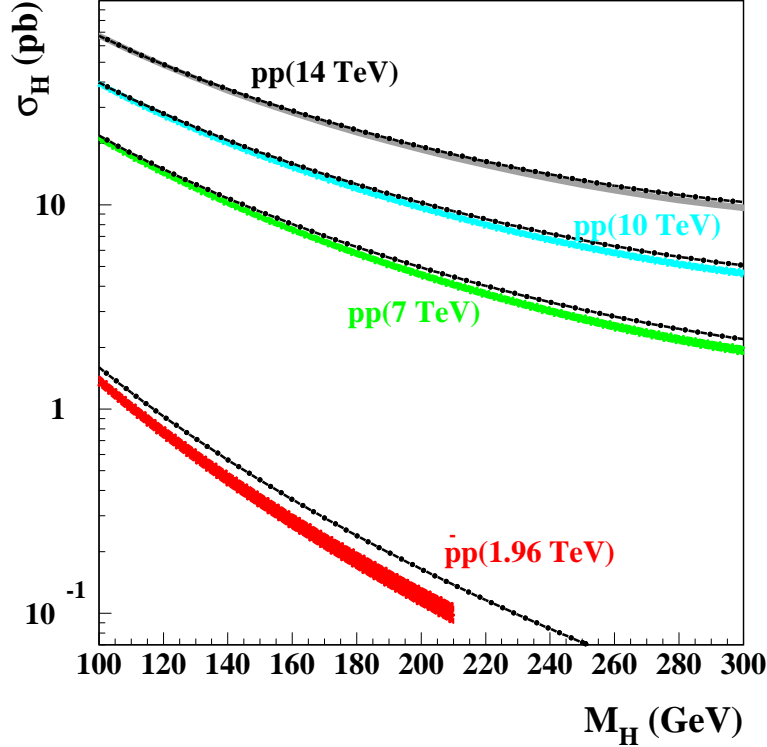


Figure 14: The $1\sigma_P$ error band for the Higgs-boson production cross sections [pb] at Tevatron and the LHC at the scale $\mu = M_H$ employing the PDFs from the present analysis (shaded area) in comparison with the central values for the case of PDFs of Ref. [47] (dash-dotted lines).

potential high-luminosity measurements planned at future facilities like EIC [68], requiring an excellent control in the *systematics*, may provide future challenges to the precision on the theoretical side.

We have discussed the NNLO PDFs of the present fit and compared to other global analyses. A comparison to the results of MSTW08 in the region $\mu^2 = 4$ to 10^4 GeV^2 show that smaller values for the light PDFs for lower values of x are obtained in Ref. [47]. Moreover, the gluon distribution of Ref. [47] at low scales $\mu^2 = 4$ GeV^2 does strongly deviate from ours turning to negative values at $x \sim 5 \cdot 10^{-5}$. At large values of x the gluon distribution of Ref. [47] is slightly larger than ours. Somewhat smaller values are also obtained for the c - and b -quark distributions. The PDFs obtained in Ref. [45] agree very well with the results of the present analysis.

We have illustrated the implications of the PDFs for standard candle processes, such as W^\pm - and Z -boson production at hadron colliders. Comparison to MSTW08 yields a $2\sigma_P$ lower result for Tevatron and better agreement is obtained for the LHC energies. Conversely, the inclusive $t\bar{t}$ production cross section of both analyses agree at Tevatron energies, but for the LHC larger results by $\sim 2\sigma_P$ are obtained with MSTW08. For the inclusive Higgs-boson production cross section at Tevatron the PDFs of MSTW08 yield a $3\sigma_P$ larger value in the whole mass range, while for LHC energies both predictions agree for masses $M_H \sim 100$ GeV , and MSTW08 gives by $3\sigma_P$ larger

values for $M_H \sim 300$ GeV. Of course, all observed differences have to be considered in view of the statistical and systematic accuracies finally to be obtained in the experimental measurements.

The PDFs of the present analysis allow for detailed simulations of the different inclusive processes at the LHC and are of central importance in monitoring the luminosity. Precision measurements of inclusive processes at hadron colliders open up the opportunity to further refine the understanding of the PDFs of nucleons. This applies to both, the final analyses at Tevatron and the future measurements at the LHC. During the last years our understanding of PDFs has steadily improved at the NNLO level and upcoming high luminosity data from hadron colliders will continue in this direction.

Grids, which allow fast access to our 3-, 4-, and 5-flavor PDFs in a wide range of x and Q^2 (including the PDF uncertainties considered) are available online at [69].

Acknowledgments.

We would like to thank P. Nadolsky, D. Renner, E. Reya, J. Smith, W.J. Stirling and R. Thorne for discussions. This work was supported in part by DFG Sonderforschungsbereich Transregio 9, Computergestützte Theoretische Teilchenphysik, the RFBR grant 08-02-91024, Studienstiftung des Deutschen Volkes, the European Commission MRTN HEPTOOLS under Contract No. MRTN-CT-2006-035505.

References

- [1] A. Aktas *et al.* [H1 collaboration], Eur. Phys. J. C **45** (2006) 23 [arXiv:hep-ex/0507081].
- [2] S. Chekanov *et al.* [ZEUS collaboration], Phys. Rev. D **69** (2004) 012004 [arXiv:hep-ex/0308068].
- [3] S. Moch, J. A. M. Vermaseren and A. Vogt, Nucl. Phys. B **688** (2004) 101 [arXiv:hep-ph/0403192];
A. Vogt, S. Moch and J. A. M. Vermaseren, Nucl. Phys. B **691** (2004) 129 [arXiv:hep-ph/0404111].
- [4] E. B. Zijlstra and W. L. van Neerven, Nucl. Phys. B **383** (1992) 525;
S. Moch and J. A. M. Vermaseren, Nucl. Phys. B **573** (2000) 853 [arXiv:hep-ph/9912355].
- [5] E. Witten, Nucl. Phys. B **104** (1976) 445;
J. Babcock, D. W. Sivers and S. Wolfram, Phys. Rev. D **18** (1978) 162;
J. P. Leveille and T. J. Weiler, Nucl. Phys. B **147** (1979) 147;
M. Glück, E. Hoffmann and E. Reya, Z. Phys. C **13** (1982) 119.
- [6] M. A. Shifman, A. I. Vainshtein and V. I. Zakharov, Nucl. Phys. B **136** (1978) 157 [Yad. Fiz. **27** (1978) 455].
- [7] E. Laenen, S. Riemersma, J. Smith and W. L. van Neerven, Nucl. Phys. B **392** (1993) 162;
ibid. 229;
S. Riemersma, J. Smith and W. L. van Neerven, Phys. Lett. B **347** (1995) 143 [arXiv:hep-ph/9411431].
- [8] I. Bierenbaum, J. Blümlein and S. Klein, Nucl. Phys. **B820** (2009) 417 [arXiv:0904.3563 [hep-ph]].
- [9] M. A. G. Aivazis, J. C. Collins, F. I. Olness and W. K. Tung, Phys. Rev. D **50** (1994) 3102 [arXiv:hep-ph/9312319].
- [10] R.S. Thorne and W.K. Tung, in: Proceedings of the workshop: HERA and the LHC workshop series on the implications of HERA for LHC physics, eds. H. Jung *et al.*, arXiv:0903.3861 [hep-ph].
- [11] M. Glück, E. Reya and M. Stratmann, Nucl. Phys. B **422** (1994) 37.
- [12] M. Buza, Y. Matiounine, J. Smith and W. L. van Neerven, Eur. Phys. J. C **1** (1998) 301 [arXiv:hep-ph/9612398];
A. Chuvakin and J. Smith, Comput. Phys. Commun. **143** (2002) 257 [arXiv:hep-ph/0103177].
- [13] I. Bierenbaum, J. Blümlein and S. Klein, Phys. Lett. B **672** (2009) 401 [arXiv:0901.0669 [hep-ph]].

- [14] M. Dittmar *et al.*, arXiv:hep-ph/0511119;
S. Alekhin *et al.*, arXiv:hep-ph/0601012.
- [15] B. W. Harris, J. Smith and R. Vogt, Nucl. Phys. B **461** (1996) 181 [arXiv:hep-ph/9508403].
- [16] S. I. Alekhin and J. Blümlein, Phys. Lett. B **594** (2004) 299 [arXiv:hep-ph/0404034].
- [17] M. Buza, Y. Matiounine, J. Smith, R. Migneron and W. L. van Neerven, Nucl. Phys. B **472** (1996) 611 [arXiv:hep-ph/9601302].
- [18] I. Bierenbaum, J. Blümlein and S. Klein, Phys. Lett. B **648** (2007) 195 [arXiv:hep-ph/0702265]; Nucl. Phys. B **780** (2007) 40 [arXiv:hep-ph/0703285].
- [19] J. Blümlein, A. De Freitas, W. L. van Neerven and S. Klein, Nucl. Phys. B **755** (2006) 272 [arXiv:hep-ph/0608024].
- [20] I. Bierenbaum, J. Blümlein, S. Klein and C. Schneider, Nucl. Phys. B **803** (2008) 1 [arXiv:0803.0273 [hep-ph]].
- [21] J. A. M. Vermaseren, A. Vogt and S. Moch, Nucl. Phys. B **724** (2005) 3 [arXiv:hep-ph/0504242] and references therein.
- [22] S. Bethke, J. Phys. G **26** (2000) R27 [arXiv:hep-ex/0004021].
- [23] R. S. Thorne and R. G. Roberts, Phys. Lett. B **421** (1998) 303 [arXiv:hep-ph/9711223].
- [24] R. S. Thorne and R. G. Roberts, Phys. Rev. D **57** (1998) 6871 [arXiv:hep-ph/9709442].
- [25] W.K. Tung, S. Kretzer and C. Schmidt, J. Phys. G **28** (2002) 983 [arXiv:hep-ph/0110247].
- [26] R.S. Thorne, Phys. Rev. D **73** (2006) 054019 [arXiv:hep-ph/0601245].
- [27] A. Chuvakin, J. Smith and W.L. van Neerven, Phys. Rev. D **61** (2000) 096004, [arXiv:hep-ph/9910250].
- [28] F.D. Aaron *et al.* [H1 Collaboration], arXiv:0907.2643 [hep-ex].
- [29] A. D. Martin, R. G. Roberts, W. J. Stirling and R. S. Thorne, Eur. Phys. J. C **28** (2003) 455 [arXiv:hep-ph/0211080].
- [30] A. Chuvakin, J. Smith and B. W. Harris, Eur. Phys. J. C **18** (2001) 547 [arXiv:hep-ph/0010350].
- [31] E. Laenen and S. O. Moch, Phys. Rev. D **59** (1999) 034027 [arXiv:hep-ph/9809550].
- [32] S. I. Alekhin and S. Moch, Phys. Lett. B **672** (2009) 166 [arXiv:0811.1412 [hep-ph]].
- [33] C. Adloff *et al.* [H1 Collaboration], Eur. Phys. J. C **21** (2001) 33 [arXiv:hep-ex/0012053].

- [34] L. W. Whitlow, E. M. Riordan, S. Dasu, S. Rock and A. Bodek, Phys. Lett. **B282**, 475 (1992);
A. C. Benvenuti *et al.* [BCDMS Collaboration], Phys. Lett. **B223** (1989) 485;
A. C. Benvenuti *et al.* [BCDMS Collaboration], Phys. Lett. **B237** (1990) 592;
M. Arneodo *et al.* [New Muon Collaboration], Nucl. Phys. **B483** (1997) 3 [hep-ph/9610231];
S. Chekanov *et al.* [ZEUS Collaboration], Eur. Phys. J. C **21**, 443 (2001)
[arXiv:hep-ex/0105090].
- [35] G. Moreno *et al.*, Phys. Rev. **D43**, 2815 (1991);
R.S. Towell *et al.* Phys. Rev. **D64**, 052002 (2001).
- [36] M. Goncharov *et al.* [NuTeV Collaboration], Phys. Rev. D **64** (2001) 112006;
A. O. Bazarko *et al.* [CCFR Collaboration], Z. Phys. C **65** (1995) 189.
- [37] S. I. Alekhin, K. Melnikov and F. Petriello, Phys. Rev. D **74** (2006) 054033.
- [38] S. I. Alekhin, S. Kulagin and R. Petti, Phys. Lett. B **675** (2009) 433;
S. I. Alekhin, Phys.Rev. **D68** (2003), 014002.
- [39] T. Gottschalk, Phys. Rev. D **23** (1981) 56;
M. Glück, S. Kretzer and E. Reya, Phys. Lett. B **380** (1996) 171 [Erratum-ibid. B **405** (1997)
391].
- [40] C. Anastasiou, L. Dixon, K. Melnikov and F. Petriello, Phys. Rev. Lett. **91** (2003), 182002;
Phys. Rev. **D69**, 094008 (2004).
- [41] B. I. Ermolaev, M. Greco and S. I. Troyan, Nucl. Phys. B **594** (2001) 71
[arXiv:hep-ph/0009037].
- [42] J. Blümlein, H. Böttcher and A. Guffanti, Nucl. Phys. B **774** (2007) 182
[arXiv:hep-ph/0607200]; Nucl. Phys. Proc. Suppl. **135** (2004) 152 [arXiv:hep-ph/0407089].
- [43] A. M. Cooper-Sarkar, arXiv:0709.0191 [hep-ph].
- [44] P. M. Nadolsky and W. K. Tung, arXiv:0903.2667 [hep-ph].
- [45] P. Jimenez-Delgado and E. Reya, Phys. Rev. D **79** (2009) 074023 [arXiv:0810.4274 [hep-
ph]].
- [46] A. D. Martin, W. J. Stirling, R. S. Thorne and G. Watt, arXiv:0905.3531 [hep-ph].
- [47] A. D. Martin, W. J. Stirling, R. S. Thorne and G. Watt, arXiv:0901.0002 [hep-ph].
- [48] H1 collaboration, Measurement of the Longitudinal Structure Function F_L of the Proton
at Low x in an extended Q^2 range, H1prelim-09-044, DIS 2009, Madrid, April 2009, Fig-
ure 17.
- [49] S. Chekanov *et al.* [ZEUS Collaboration], Eur. Phys. J. C **42** (2005) 1
[arXiv:hep-ph/0503274].

- [50] P. M. Nadolsky *et al.*, Phys. Rev. D **78** (2008) 013004 [arXiv:0802.0007 [hep-ph]].
- [51] R. D. Ball *et al.* [NNPDF Collaboration], Nucl. Phys. B **809** (2009) 1 [Erratum-ibid. B **816** (2009) 293] [arXiv:0808.1231 [hep-ph]].
- [52] D. Renner, Proc. of the Int. Conference LATTICE 2009 and references therein, to appear.
- [53] R. Hamberg, W. L. van Neerven and T. Matsuura, Nucl. Phys. B **359** (1991) 343 [Erratum-ibid. B **644** (2002) 403].
- [54] R. V. Harlander and W. B. Kilgore, Phys. Rev. Lett. **88** (2002) 201801 [arXiv:hep-ph/0201206].
- [55] S. Catani, L. Cieri, G. Ferrera, D. de Florian and M. Grazzini, arXiv:0903.2120 [hep-ph].
- [56] J. Blümlein and V. Ravindran, Nucl. Phys. B **716** (2005) 128 [arXiv:hep-ph/0501178].
- [57] M. Dittmar, F. Pauss and D. Zurcher, Phys. Rev. D **56** (1997) 7284 [arXiv:hep-ex/9705004].
- [58] P. Nason, S. Dawson and R. K. Ellis, Nucl. Phys. B **303**, 607 (1988).
- [59] W. Beenakker, H. Kuijf, W. L. van Neerven and J. Smith, Phys. Rev. D **40**, 54 (1989).
- [60] W. Bernreuther, A. Brandenburg, Z. G. Si and P. Uwer, Nucl. Phys. B **690**, 81 (2004) [arXiv:hep-ph/0403035].
- [61] M. Czakon and A. Mitov, arXiv:0811.4119 [hep-ph].
- [62] S. Moch and P. Uwer, Phys. Rev. D **78** (2008) 034003 [arXiv:0804.1476 [hep-ph]].
- [63] U. Langenfeld, S. Moch and P. Uwer, arXiv:0906.5273 [hep-ph].
- [64] P. M. Nadolsky *et al.*, Phys. Rev. D **78**, 013004 (2008) [arXiv:0802.0007 [hep-ph]].
- [65] C. Anastasiou and K. Melnikov, Nucl. Phys. B **646** (2002) 220 [arXiv:hep-ph/0207004].
- [66] V. Ravindran, J. Smith and W. L. van Neerven, Nucl. Phys. B **665** (2003) 325 [arXiv:hep-ph/0302135].
- [67] S. Catani and M. Grazzini, Phys. Rev. Lett. **98** (2007) 222002 [arXiv:hep-ph/0703012].
- [68] C. Aidala *et al.* A High Luminosity, High Energy Electron-Ion-Collider, A White Paper Prepared for the NSAC LRP 2007.
- [69] <https://mail.ihep.ru/~alekhin/pdfs.html>